OAK RIDGE NATIONAL LABORATORY
operated by
UNION CARBIDE CORPORATION
NUCLEAR DIVISION
for the
U.S. ATOMIC ENERGY COMMISSION

ORNL-TM-3105

COPY NO. -

DATE - August 24, 1970

Neutron Physics Division

THE ABSORBED DOSE AND DOSE EQUIVALENT FROM NEGATIVELY AND POSITIVELY CHARGED PIONS IN THE ENERGY RANGE 10 TO 2000 MeV*

R. G. Alsmiller, Jr., T. W. Armstrong,
and Barbara L. Bishop

Abstract

Nucleon-meson cascade calculations have been carried out for broad beams of monoenergetic negatively and positively charged pions normally incident on a semi-infinite slab of tissue 30-cm thick, and the absorbed doses and dose equivalents as a function of depth in the tissue are presented. Results are given for incident energies of 10, 30, 84, 150, 500, 1000, and 2000 MeV. For the lower incident energies ($\leq$ 84 MeV), the pion range is < 30 cm in tissue, and peaks in the absorbed doses and dose equivalents, due to the reaction products produced by the nuclear capture of the stopped negatively charged pions and to the decay products of the stopped positively charged pions, are clearly evident.

NOTE: This Work Partially Funded by
NATIONAL AERONAUTICS AND SPACE ADMINISTRATION
Under Order H-38280A

*Submitted for journal publication.

I. INTRODUCTION

In a previous paper,[1] hereinafter referred to as paper 1, the calculated absorbed doses and dose equivalents from broad beams of high-energy (< 3000 MeV) neutrons and protons were presented. In the present paper, calculated results for the case of broad beams of incident negatively and positively charged pions are presented. The results are of interest not only because of their applicability in the shielding of high-energy accelerators but also because of the possible use of negatively charged pions in cancer radiotherapy.[2-4] Since the results presented here are for the case of incident beams of infinite width, they do not apply directly to cancer therapy; that is, in cancer therapy the lateral spread of narrow beams of negatively charged pions is of importance. The results do, however, include reliable estimates of the absorbed dose and dose equivalent produced by the reaction products that arise from the nuclear capture of negative pions which come to rest in tissue.

In Sec. II the method of calculation is discussed. In Sec. III the calculated results are presented and discussed.

II. METHOD OF CALCULATION

The method of calculation and the cross-section data used in obtaining the results presented in this paper are in almost all respects the same as those used in paper 1. The only notable difference between the calculational method used here and that used in paper 1 is that here the electrons and positrons from muon decay are transported, while in paper 1 these particles were assumed to deposit their energy at their point of origin. The method used to transport electrons and positrons is described later in this section. All of the results were obtained using the nucleon-meson transport code

written by Coleman.[5] The code is described in some detail in ref. 5, but, for completeness, a description of the physical interactions that are included in the present calculations is given here.

Charged-Particle Energy Loss

The energy loss of protons, charged pions, and muons by the excitation and ionization of atomic electrons is treated in the continuous slowing-down approximation using the well-established energy loss per unit distance of such particles.[5,6] The density-effect correction to the energy loss of all charged particles has been calculated using the asymptotic form of the correction.[7]

Nucleon-Nucleus and Pion-Nucleus Nonelastic Collisions

At energies > 15 MeV for nucleons and > 2.2 MeV for charged pions,[5] the differential cross sections for nucleon and pion emission from nucleon-nucleus and pion-nucleus nonelastic collisions are obtained from the intranuclear-cascade-evaporation model of nuclear reactions.[8-10] This model gives the energy and angular distribution of the emitted nucleons and pions. The evaporation portion of the intranuclear-cascade-evaporation calculations is carried out with the version of the code EVAP-3,[11] which is suitable for use with the intranuclear-cascade code of Bertini.[8,9] This evaporation code gives an estimate of the energy of the emitted deuterons, tritons, ^{3}He's, alpha particles, and photons, as well as an estimate of the kinetic energy of the recoiling residual nucleus from a nonelastic collision.

The differential cross sections for particle production from nucleon and pion nonelastic collisions with hydrogen nuclei are the same as those used in the intranuclear-cascade calculations of Bertini.[8-10,12]

Proton-nucleus nonelastic collisions below 15 MeV and pion-nucleus nonelastic collisions below 2.2 MeV (except forth e capture of negative pions at rest) are neglected. Particle production from neutron-nucleus nonelastic collisions below 15 MeV is obtained using the code EVAP-3 as described in ref. 11 in conjunction with the total nonelastic cross-section data on the 05R master cross-section tape.[a]

Nucleon-Nucleus and Pion-Nucleus Elastic Collisions

The elastic collisions of protons and pions with all nuclei other than hydrogen are neglected. The differential cross sections for the elastic collision of neutrons with nuclei other than hydrogen are those given on the 05R master cross-section tape.[a] The differential cross sections for the elastic collisions of nucleons with energy > 15 MeV and pions with energy > 2.2 MeV with hydrogen nuclei are taken from experimental data and are the same as those used in the intranuclear-cascade calculations of Bertini.[8,9,12] The differential cross sections for the elastic collisions of neutrons with energy < 15 MeV with hydrogen nuclei are those given on the 05R master cross-section tape.[a]

Charged-Pion Decay in Flight

Charged pions are unstable and may decay into muons and neutrinos. Charged-pion decay in flight is taken into account using the known pion lifetime. When a decay occurs, the energy and angular distribution of the produced muon is obtained by assuming that the decay is isotropic in the rest frame of the pion and by using the Lorentz transformation to transform the distribution from the pion rest frame into the laboratory system. The produced neutrino deposits no energy in the tissue and is therefore of no interest here.

Charged-Pion Decay and Capture at Rest

Charged pions may come to rest in the tissue. When a positively charged pion comes to rest, it will ultimately decay into a positively charged muon and a neutrino, and the energy and angular distribution of the muon may be obtained in the same manner as when a positively charged muon decays in flight (see above). When a negatively charged pion comes to rest, it usually will not decay but will be captured by a nucleus and will produce a variety of secondary particles. In the calculations reported here, it is assumed that all negatively charged pions that come to rest are captured, and the energy and angular distribution of the particles produced as a result of this capture is obtained from the intranuclear-cascade-evaporation model of nuclear reactions, since it has previously been shown that this model describes the capture process quite well.[13]

Neutral-Pion Decay

The neutral pion is very unstable and for practical purposes may be assumed to decay into two photons at its point of origin. The two photons have equal and opposite momenta in the rest system of the pion, and the sum of their energies in this system is equal to the pion rest energy. The energy and angular distribution of the photons in the laboratory system is obtained by assuming that the decay is isotropic in the rest system of the pion and by using the Lorentz transformation to transform from the rest system to the laboratory system.

Muon Decay in Flight and at Rest

Muons are unstable and may decay into electrons or positrons, depending on the charge of the muons, and neutrinos. Muon decay in flight is taken into account using the known muon lifetime, and muons which come to

rest are assumed to decay. The energy and angular distribution of the electron or positron in the muon rest system is known,[14] and the energy and angular distribution of these particles in the laboratory system is obtained by using the Lorentz transformation. In the work reported here, the asymmetric portion of the energy and angular distribution in the muon rest system due to the polarization of the muon has been neglected; that is, the angular distribution of the electron or positron in the muon rest system has been taken to be isotropic.[14]

Electron-Photon Cascade From High-Energy Photons, Electrons, and Positrons

Photons from the decay of neutral pions, and electrons and positrons from the decay of muons are relatively high in energy, and in passing through matter they induce an electron-photon cascade. To obtain the energy deposited by such cascades, results obtained from the cascade code written by Zerby and Moran[15-18] and the published results of Beck[19] and Claiborne and Trubey[20] were used. The procedure followed was to construct curves of energy deposition as a function of depth and incident photon energy and to interpolate in these curves to find the energy deposited in subslabs of the tissue by each electron, positron, or photon produced in the Monte Carlo calculations. This procedure is approximate in that it does not accurately account for the lateral spread of the cascade, but the error is not thought to be large.

Thermal-Neutron Capture

Neutrons which become thermalized will be captured by hydrogen and nitrogen if they do not escape from the system. The energy deposited by the photons produced by thermal-neutron capture in hydrogen and by the protons produced by thermal-neutron capture in nitrogen is included in the calculations by using the capture cross sections from the 05R master cross-section tape.[a]

Transport Details

In the calculations reported here, neutrons, protons, charged pions, and muons are transported through the tissue taking into account the energy and angular distributions with which these particles are produced.[5] The transport of electrons and positrons from muon decay and photons from neutral pion decay is carried out using the calculated results on electron-photon cascades as described above (see page 7). Heavy nuclei, that is, nuclei with mass number greater than one, are not transported but are assumed to deposit their energy at their point of origin. This assumption is quite valid because these particles have a very short range. Photons from all nonelastic nucleon-nucleus and pion-nucleus collisions are assumed to deposit their energy at their point of origin. These photons are relatively low in energy and could be transported without difficulty if their spectrum was known, but for the higher incident nucleon and pion energies ($\gtrsim$ 15 MeV) the spectrum cannot be calculated at all well.[21] The assumption that these photons deposit their energy at their point of origin is not entirely valid but is somewhat justified here in that in most instances these photons contribute only a small amount to the absorbed dose and dose equivalent.

The geometry considered throughout this paper is that of a broad beam of monoenergetic pions normally incident on a semi-infinite slab of tissue 30-cm thick. The composition of tissue is the same as that used in the previous calculations[1,22] and is shown in Table I.

The calculation of the dose equivalent was carried out taking the quality factor to be a function of the linear energy transfer as in the previous calculations.[1] In the case of protons, the damage curve given by Turner *et al.*,[23] which is based on the recommendations of the National

TABLE I

Composition of Tissue

Element	Density of Nuclei (nuclei/cm^3)
H	6.265×10^{22}
O	2.551×10^{22}
C	9.398×10^{21}
N	1.342×10^{21}

Committee on Radiation Protection and Measurements, was used. In the case of charged pions and muons, the quality factor as a function of linear energy transfer was taken to be the same as that for protons, and damage curves for charged pions and muons, constructed in a manner similar to the proton damage curve given in ref. 23, were used. A quality factor of 20 was assigned to the energy deposited by all heavy nuclei and a quality factor of unity was assigned to the energy deposited by electrons, positrons, and photons.

III. RESULTS AND DISCUSSION

Calculations have been carried out for incident negatively and positively charged pions with energies of 10, 30, 84, 150, 500, 1000, and 2000 MeV.

In Figs. 1 and 2 the contribution to the absorbed dose and dose equivalent, respectively, from the various kinds of particles produced in tissue by 84-MeV incident negatively charged pions is shown.[b] The total absorbed dose and the total dose equivalent are obtained by adding all of the contributions in each figure. In Fig. 1 the histogram labeled "primary ionization" gives the absorbed dose from the ionization and excitation of atomic electrons by those incident pions that have not undergone nuclear interaction. The histogram labeled "secondary protons" gives the absorbed dose from the excitation and ionization of atomic electrons by protons produced from nonelastic nucleon-nucleus and pion-nucleus collisions and from the elastic collisions of nucleons and pions with hydrogen nuclei. The histogram labeled "heavy nuclei" gives the absorbed dose from particles with mass number > 1 produced from nonelastic nucleon-nucleus and pion-nucleus collisions and the absorbed dose from the recoiling nuclei produced from elastic neutron-nucleus collisions and from nonelastic nucleon-nucleus and

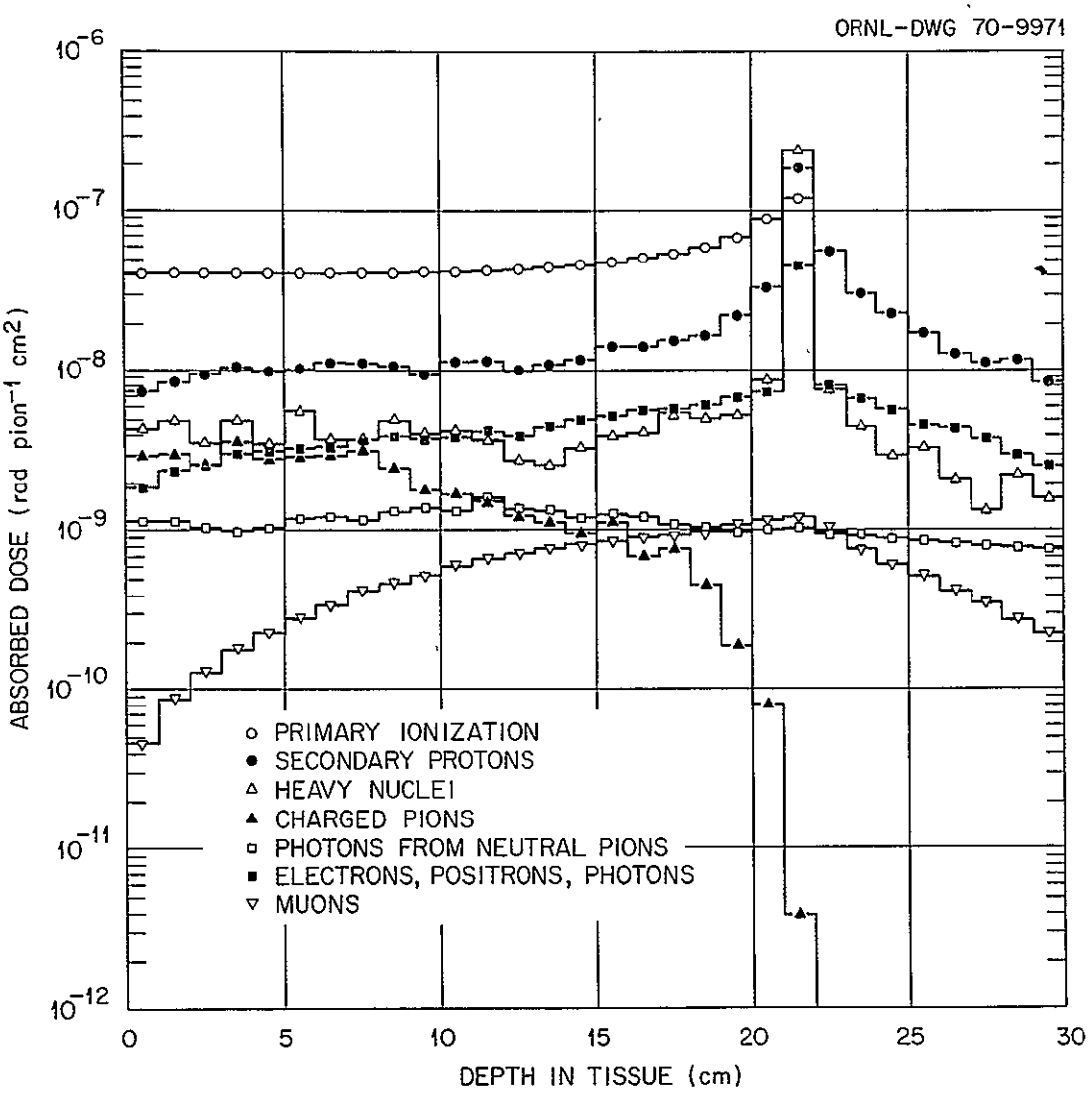

Fig. 1. Absorbed Dose from the Various Kinds of Particles vs Depth in Tissue for 84-MeV Normally Incident Negatively Charged Pions.

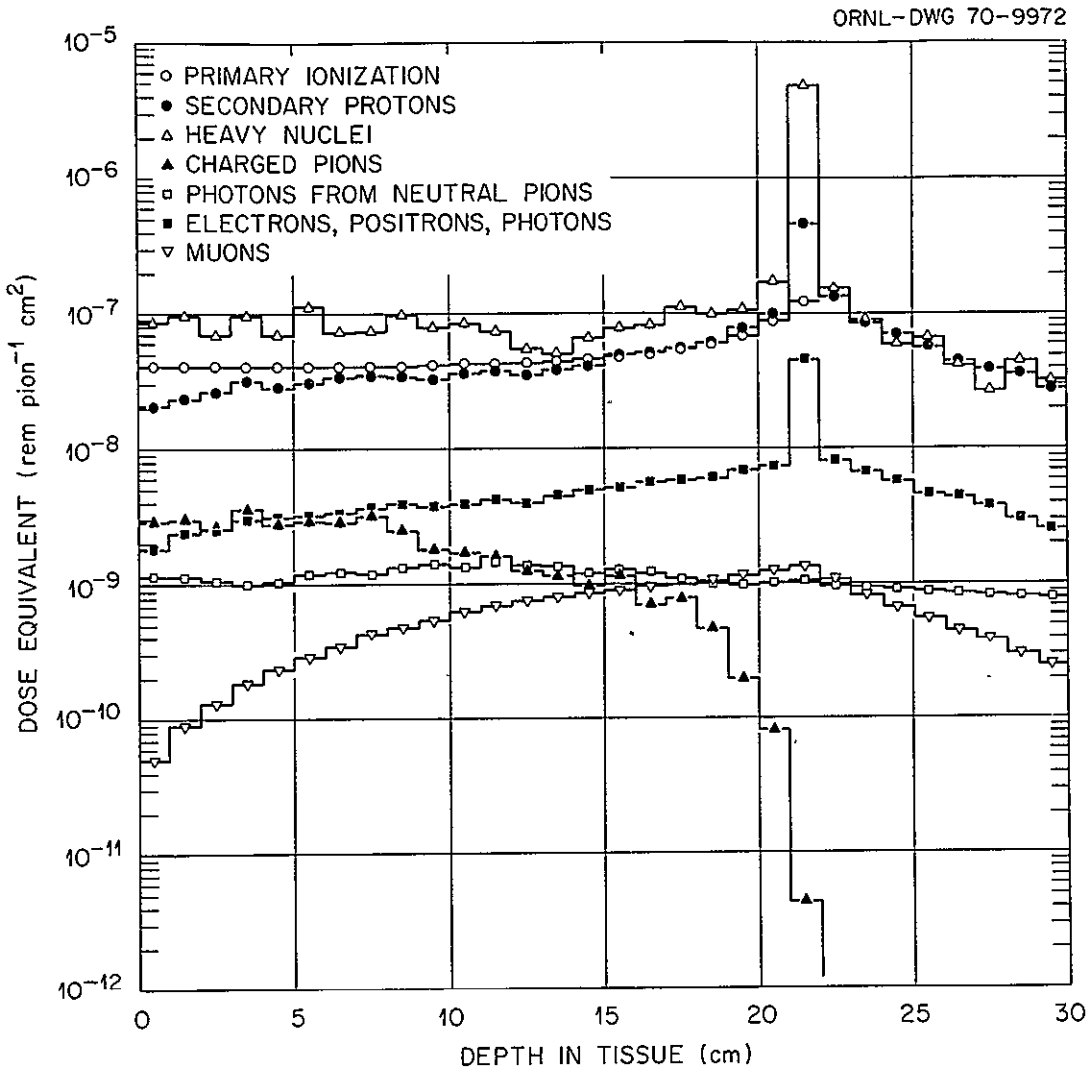

Fig. 2. Dose Equivalent from the Various Kinds of Particles vs Depth in Tissue for 84-MeV Normally Incident Negatively Charged Pions.

pion-nucleus collisions. The histogram labeled "charged pions" gives the absorbed dose from the excitation and ionization of atomic electrons by both negatively and positively charged pions produced from nuclear interactions. The histogram labeled "photons from neutral pions" gives the absorbed dose from the electron-photon cascade produced by the photons that arise from the decay of neutral pions. The histogram labeled "electrons, positrons, and photons" gives the absorbed dose from the electrons and positrons that arise from the decay of muons and the absorbed dose from the photons produced from nonelastic nucleon-nucleus and pion-nucleus collisions. The histogram labeled "muons" gives the absorbed dose from the ionization and excitation of atomic electrons by both negatively and positively charged muons. In Fig. 2 the histograms have similar meanings but give the dose equivalents from the various kinds of particles.

The range of 84-MeV pions in tissue is between 21 and 22 cm, and therefore the primary-ionization histogram in Fig. 1 does not extend beyond 22 cm. The increase in the absorbed dose from the primary particles near the end of their range is due to the increase in the pion stopping power as the pion energy decreases. The peaks in the absorbed doses from secondary protons, heavy nuclei, and photons at the end of the pion range arise from the particles that are produced by the nuclear capture of the negative pions which come to rest. A large fraction of the pion rest energy is converted by the capture process into charged particles (protons and heavy nuclei) which have a sufficiently short range that they deposit their energy in the immediate vicinity of the capture event. The peak in the histogram labeled "electrons, positrons, and photons" is primarily due to photons produced in the capture process. This photon peak is overestimated somewhat in the

present calculations because these photons, that is, photons produced by nonelastic collisions, are assumed to deposit all of their energy at their point of origin.

In Fig. 2 the peaks in the dose-equivalent histograms at a depth of 21 to 22 cm have the same origin as the corresponding peaks in Fig. 1. In Fig. 2, however, the peak in the dose equivalent from heavy nuclei is more pronounced because of the large quality factor which is attributed to heavy nuclei. It is, of course, the ability of negative pion beams to produce a large dose equivalent in a small spatial region that seems to make them ideally suited for cancer radiotherapy. It should be noted that in both Figs. 1 and 2 the magnitudes of the peaks are determined by the somewhat arbitrary 1-cm spatial interval over which the doses have been averaged; that is, the shape of the dose equivalents within the 1-cm interval has not been determined. It should also be noted that pion range straggling, which has been neglected in the calculations presented here, is probably not a negligible effect in the vicinity of peaks such as those shown in Figs. 1 and 2. In Fig. 1 there is an appreciable contribution to the absorbed dose from secondary protons at all depths. In fact, beyond the pion range the major contribution to the absorbed dose is from secondary protons. In Fig. 2 there is an appreciable contribution to the dose equivalent from secondary protons and heavy nuclei at all depths.

In Figs. 3 and 4 the contribution to the absorbed dose and dose equivalent from the various kinds of particles produced in tissue by 84-MeV incident positively charged pions are shown. The meanings of the various histograms in these figures are the same as those in Figs. 1 and 2. The pion range is between 21 and 22 cm and therefore in Figs. 3 and 4, as in

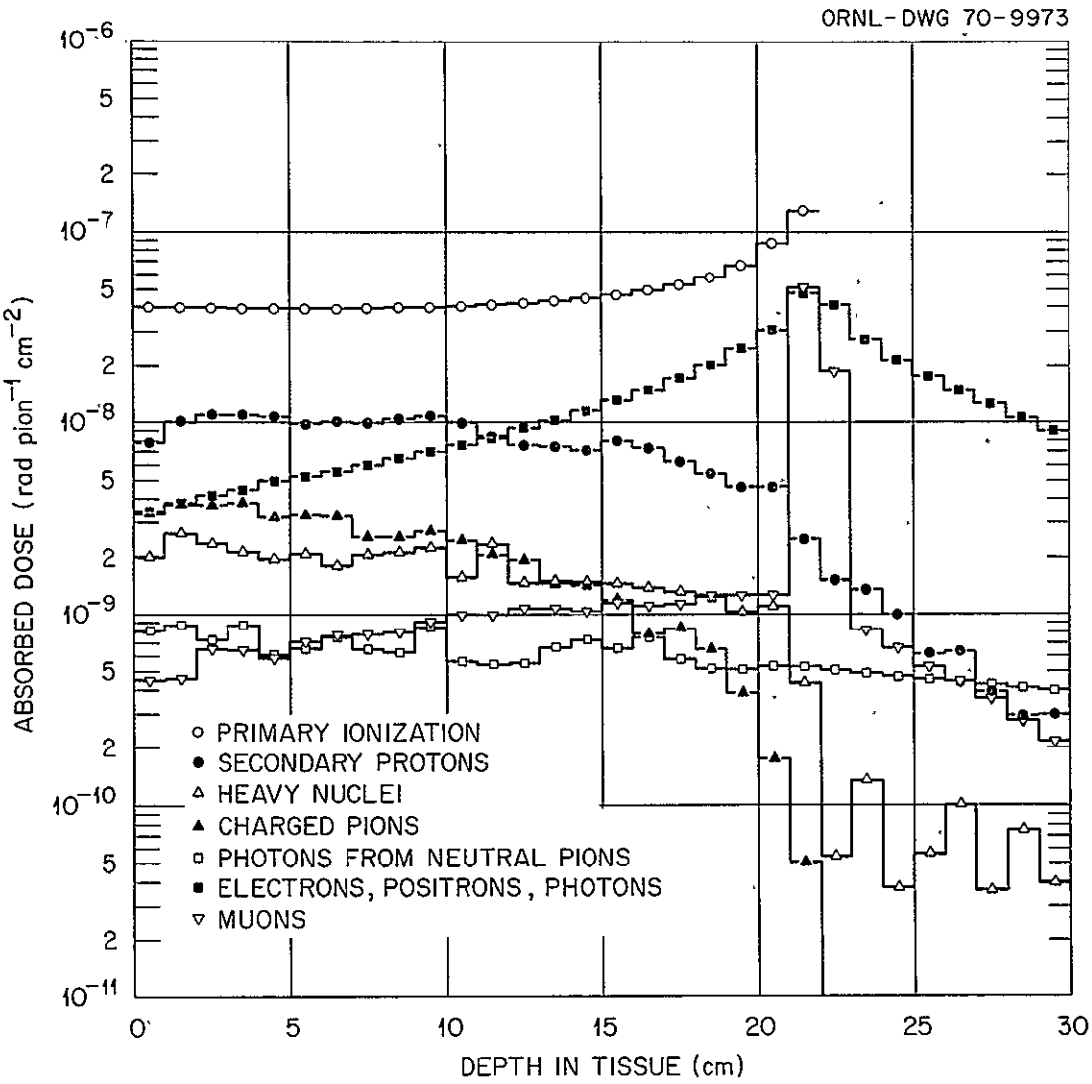

Fig. 3. Absorbed Dose from the Various Kinds of Particles vs Depth in Tissue for 84-MeV Normally Incident Positively Charged Pions.

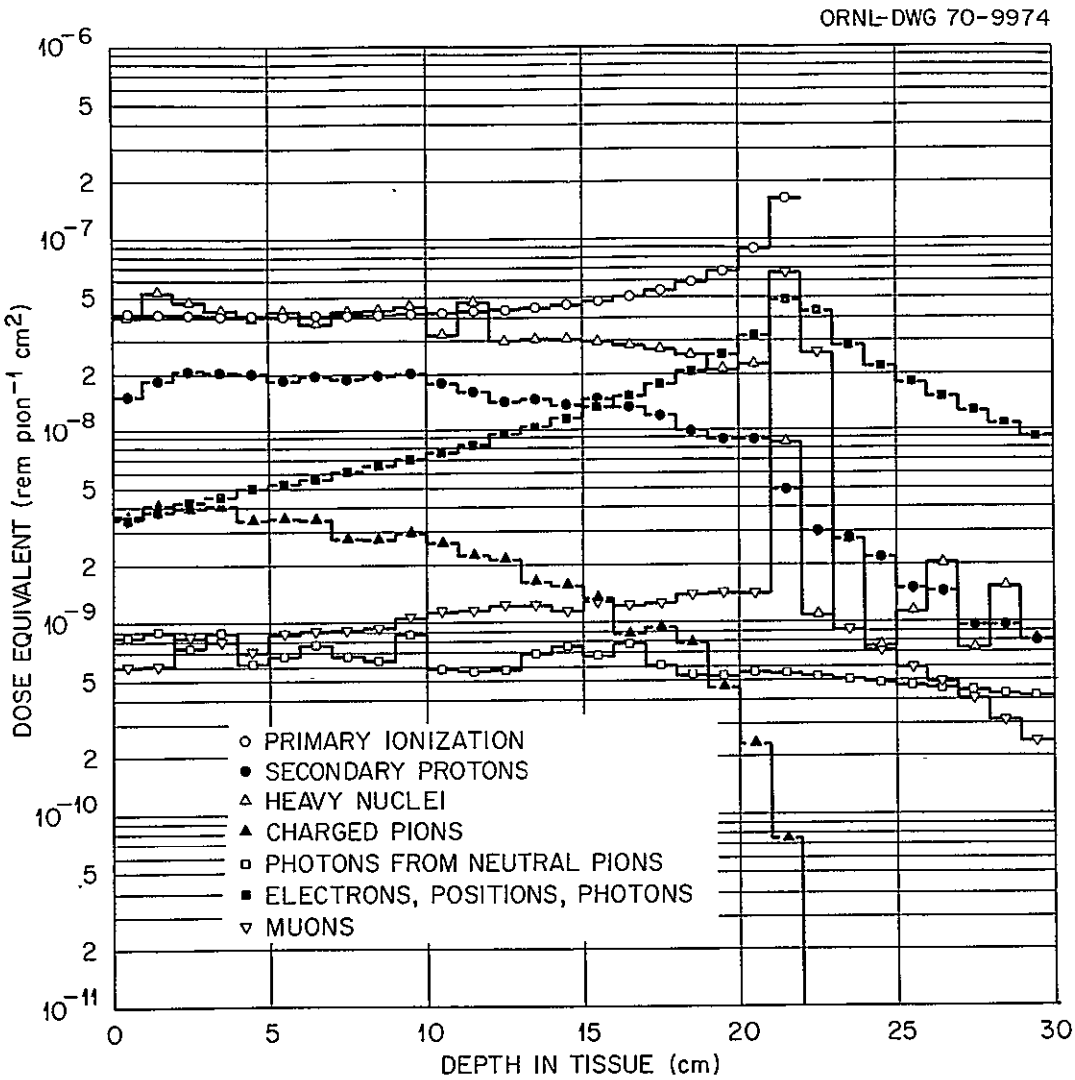

Fig. 4. Dose Equivalent from the Various Kinds of Particles vs Depth in Tissue for 84-MeV Normally Incident Positively Charged Pions.

Figs. 1 and 2, the primary ionization curve does not extend beyond 22 cm. The peaks in the histograms labeled "muons" and "electrons, positrons, and photons" in the 21- to 22-cm interval arise from the decay of these incident pions that come to rest and then decay. A positive pion at rest will decay into a positive muon with a kinetic energy of approximately 4 MeV.[25] The range of a muon with this kinetic energy is very small, and thus the muon from the decay of a stopped pion will stop and decay very near its point of origin. The positron from the decay of the positive muon will be relatively high in energy and will deposit only a small portion of its energy in the immediate vicinity of the point where the muon decays. By comparing Figs. 1 and 3, it can be seen that a larger fraction of the pion rest energy is deposited locally when a stopped negative pion is captured than when a stopped positive pion decays. Furthermore, by comparing Figs. 1 to 4, it can be seen that the energy deposited locally when a stopped negatively charged pion is captured has associated with it a much larger quality factor than the energy deposited locally when a stopped positively charged pion decays. In Fig. 3 there is an appreciable contribution to the absorbed dose at small depths, but at the larger depths the major contribution to the absorbed dose is from the electron-photon cascade produced from the positrons which arise from positive muon decay. In Fig. 4 there is an appreciable contribution to the dose equivalent at small depths from secondary protons and heavy nuclei, but the major contribution to the dose equivalent at the larger depths is that from the electron-photon cascade induced by the positrons.

In Figs. 5 and 6 the contribution to the absorbed dose and dose equivalent, respectively, from the various kinds of particles produced in tissue by 2000-MeV incident negatively charged pions is shown. In Figs. 7 and 8

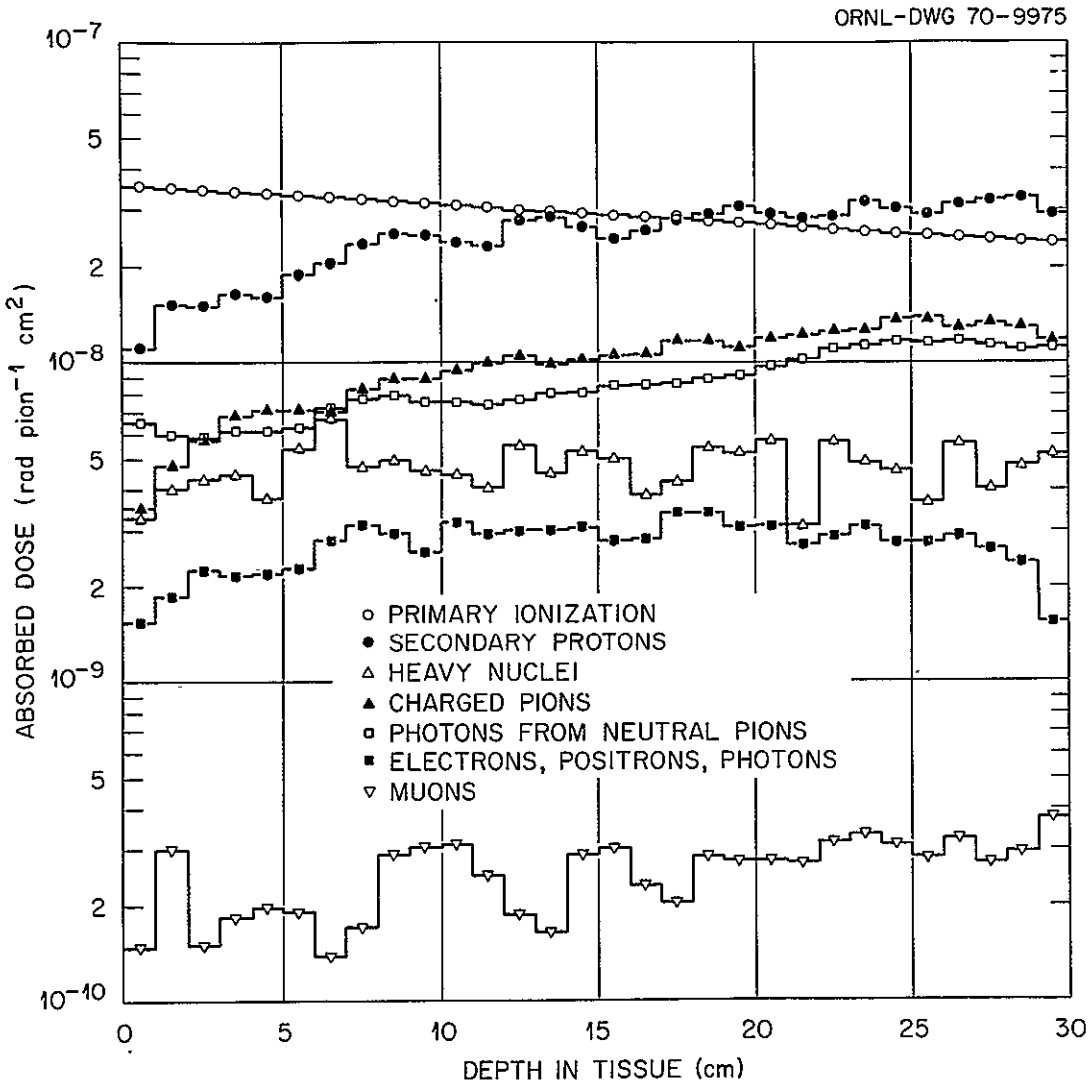

Fig. 5. Absorbed Dose from the Various Kinds of Particles vs Depth in Tissue for 2000-MeV Normally Incident Negatively Charged Pions.

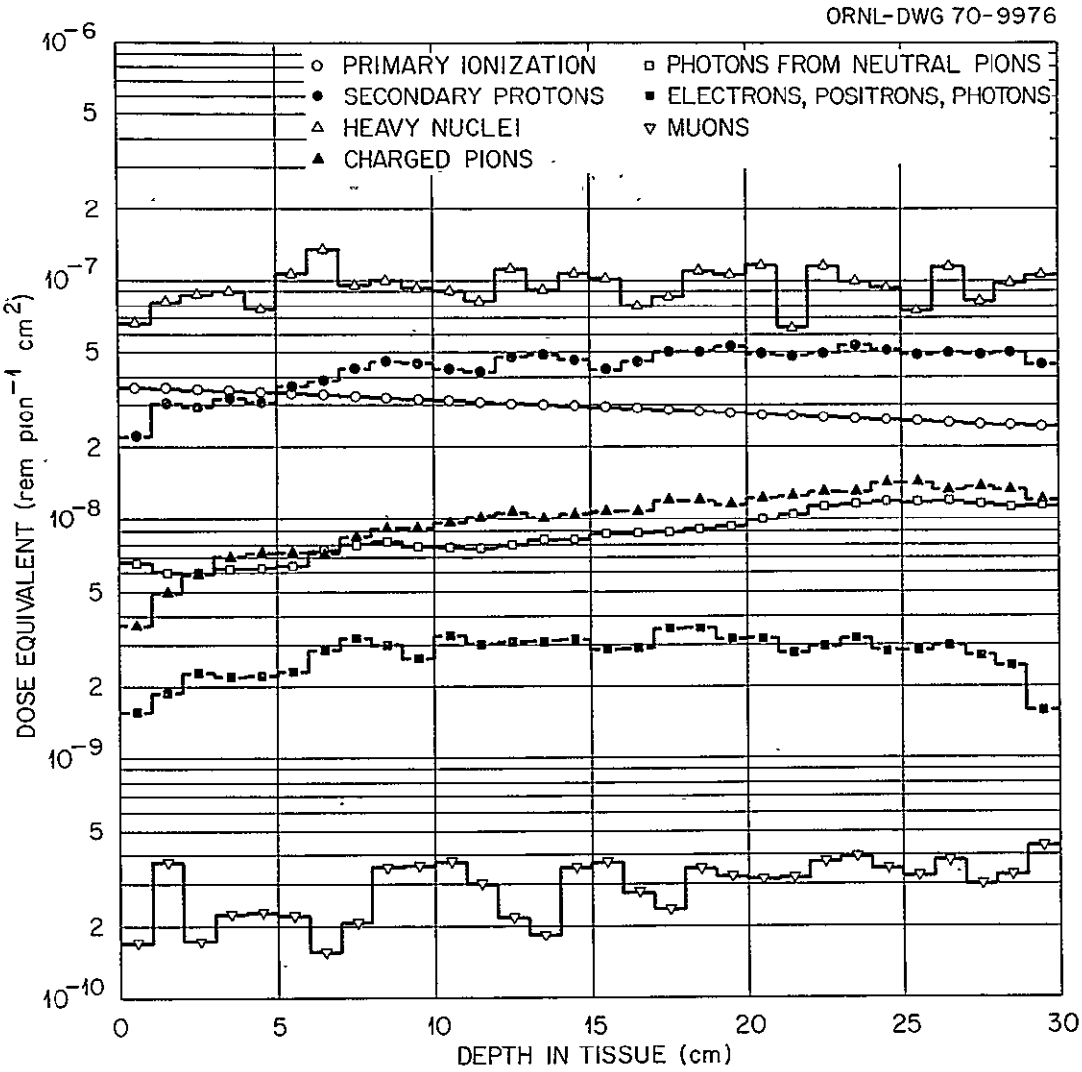

Fig. 6. Dose Equivalent from the Various Kinds of Particles vs Depth in Tissue for 2000-MeV Normally Incident Negatively Charged Pions.

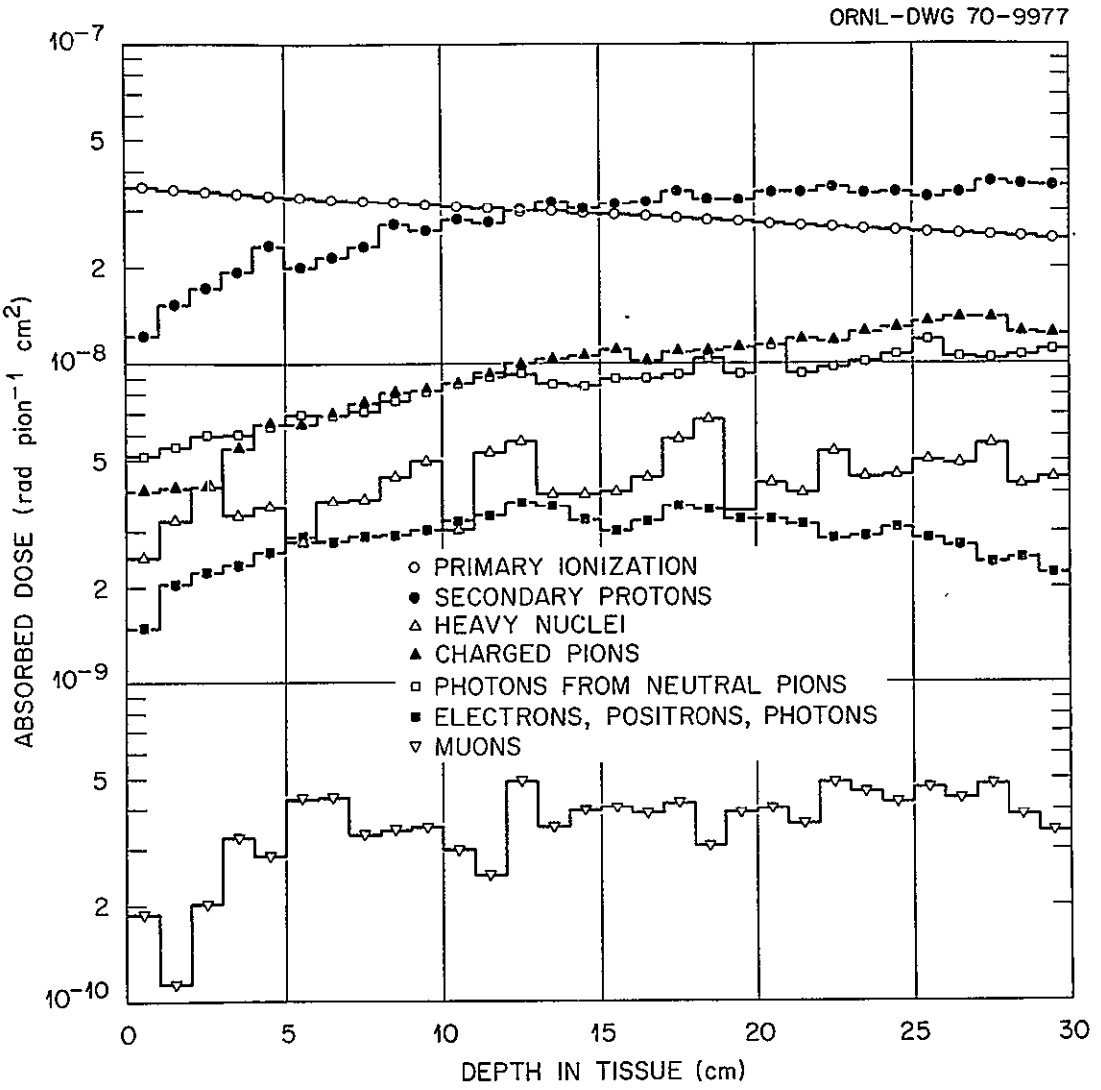

Fig. 7. Absorbed Dose from the Various Kinds of Particles vs Depth in Tissue for 2000-MeV Normally Incident Positively Charged Pions.

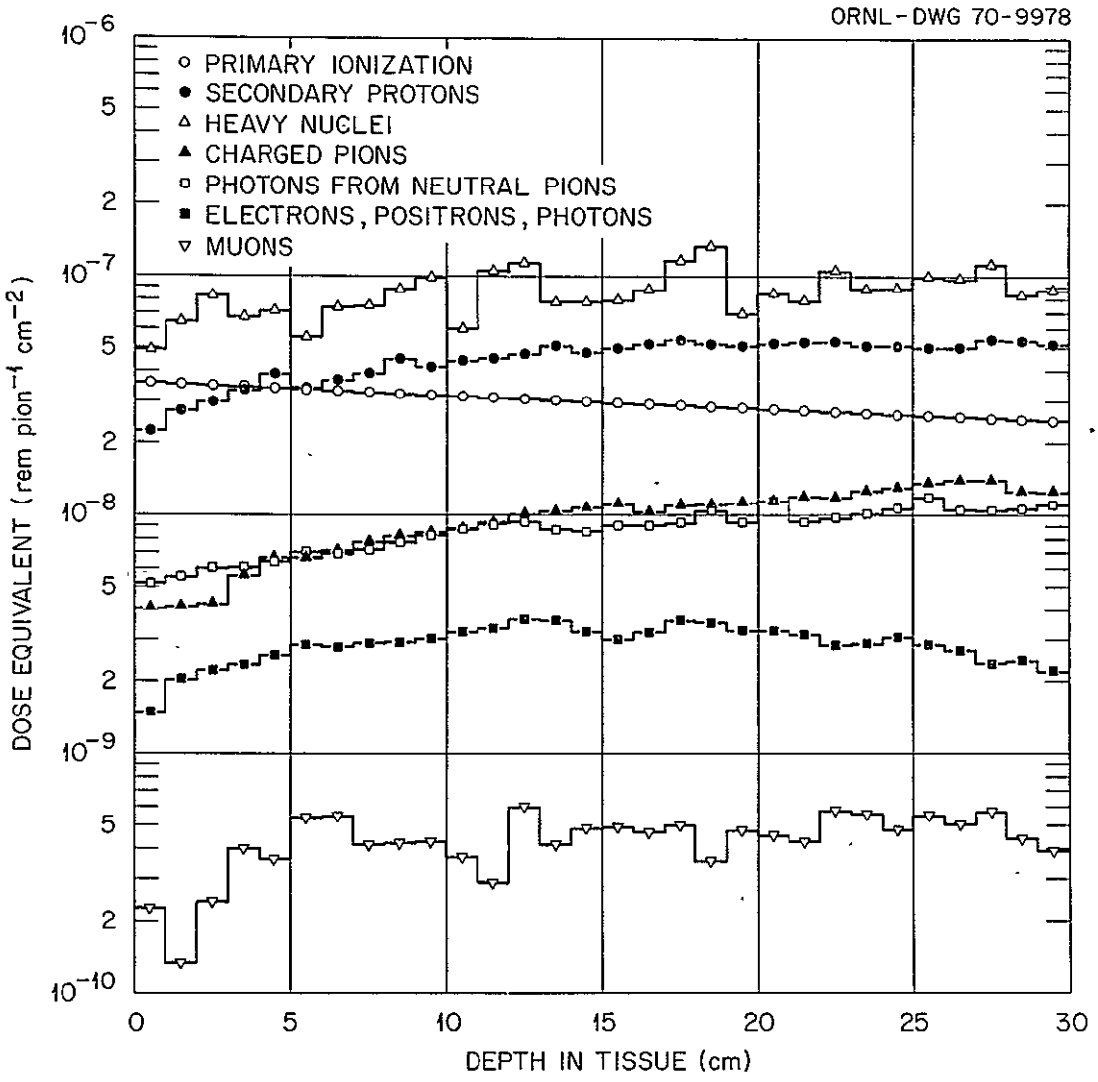

Fig. 8. Dose Equivalent from the Various Kinds of Particles vs Depth in Tissue for 2000-MeV Normally Incident Positively Charged Pions.

similar results are given for 2000-MeV incident positively charged pions.[c] At this energy, incident pions of both charges pass through the 30-cm tissue slab unless they undergo nuclear interaction, and thus there are no peaks due to stopped pions as in Figs. 1 to 4. In Figs. 5 and 7 the major contribution to the absorbed dose is from primary pion ionization and secondary protons. In Figs. 6 and 8 the dose equivalent from heavy nuclei is the largest contributor to the total dose equivalent, but there is also an appreciable contribution from primary pion ionization and from secondary protons.

In Figs. 9 and 10 the absorbed dose and dose equivalent, respectively, for all of the incident energies considered here are shown as a function of depth. In each figure, the solid-line histogram gives the results for negative pions and the dashed-line histogram gives the results for positive pions. For incident energies of 10-, 30-, and 84-MeV, the peaks in the absorbed dose and dose equivalent occur at the end of the incident pion range. In the vicinity of the peak, the absorbed dose and particularly the dose equivalent are always larger for negative pions than for positive pions. For incident energies of 30 and 84 MeV, there is no appreciable difference in the absorbed dose from positive and negative pions at the smaller depths, that is, at the depths over which the incident pions are slowing down. At incident energies of 150 MeV and above, the absorbed dose is relatively flat as a function of depth. For incident energies of 500, 1000, and 2000 MeV there is no appreciable difference between the absorbed doses from positive and negative pions, but there is a significant difference for an incident energy of 150 MeV. This difference at 150 MeV is probably due to the large difference between the π^+-proton and π^--proton elastic-scattering cross

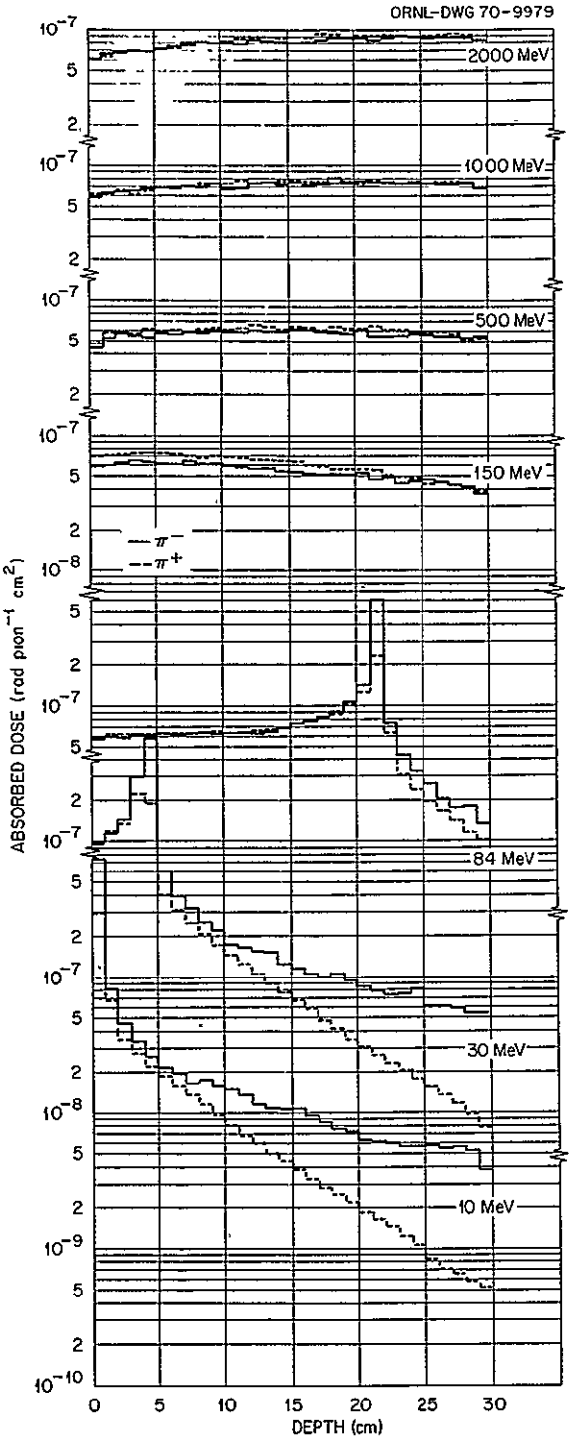

Fig. 9. Absorbed Dose vs Depth in Tissue for Monoenergetic Normally Incident Negatively and Positively Charged Pions.

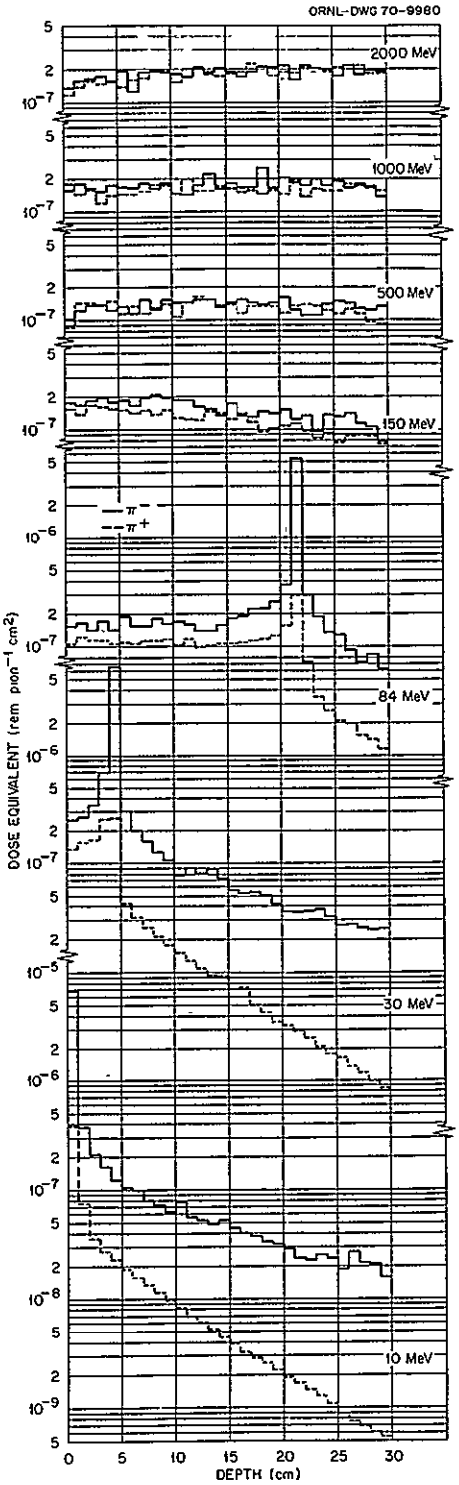

Fig. 10. Dose Equivalent vs Depth in Tissue for Monoenergetic Normally Incident Negatively and Positively Charged Pions.

sections in this energy region.[d] At the lower energies in Fig. 10, the dose equivalents from negative pions are larger at all depths than the dose equivalents from positive pions, but at the higher energies the dose equivalents from negative and positive pions are comparable at all depths.

In Fig. 11 the absorbed dose and dose equivalent averaged over the 30-cm tissue depth are shown as a function of incident energy for negatively and positively charged pions. The curves have been drawn by eye through the plotted points which give the actual calculated values. The curves have not been drawn between 84 and 150 MeV because the shape of the curves in this energy region has not been determined. A rather abrupt change may be expected to occur in the absorbed dose and dose equivalent for approximately 108-MeV incident pions because at this energy the pion range is 30 cm in tissue, and thus at slightly higher energies those pions that do not undergo nuclear collisions will pass through the slab and no part of their rest energy will be deposited in the tissue. The fact that the average dose equivalent from positive pions increases as the incident energy changes from 84 to 150 MeV is probably due to the large π^+-proton elastic-scattering cross section in the 100- to 150-MeV energy region.

For radiation protection purposes, the maximum absorbed dose and dose equivalent which occur in the 30-cm slab of tissue are often used. Therefore, in Fig. 12 the "maximum" absorbed dose and dose equivalent are shown as a function of incident pion energy for both negatively and positively charged pions. It is very important to note that for incident energies of $\leq$ 84 MeV the values shown in the figure were taken directly from Figs. 9 and 10 and therefore correspond to an average over a particular 1-cm interval. The shape of the curves in Figs. 9 and 10 in the vicinity of the

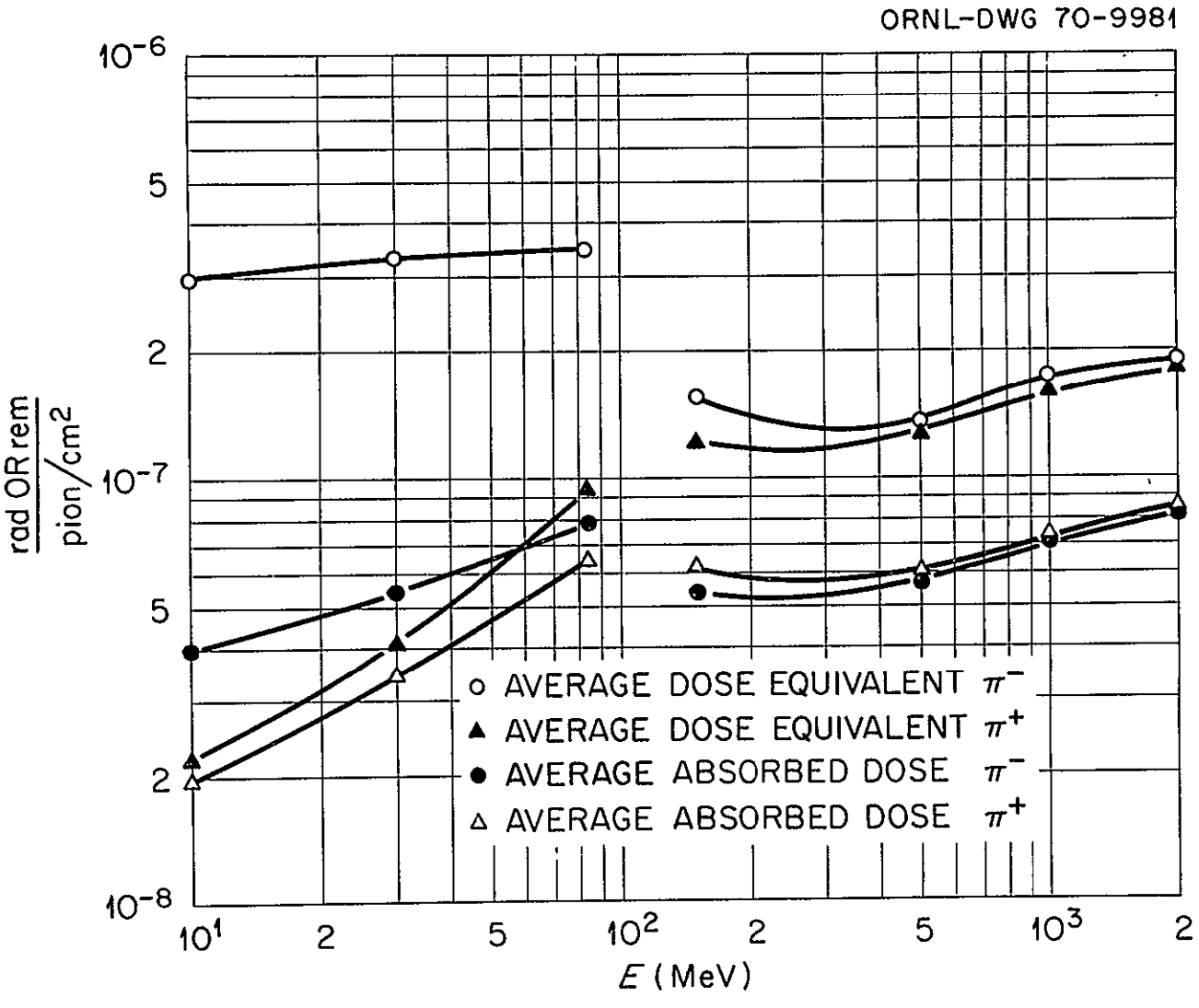

Fig. 11. Absorbed Dose and Dose Equivalent Averaged Over 30-cm Tissue Depth vs Incident Pion Energy.

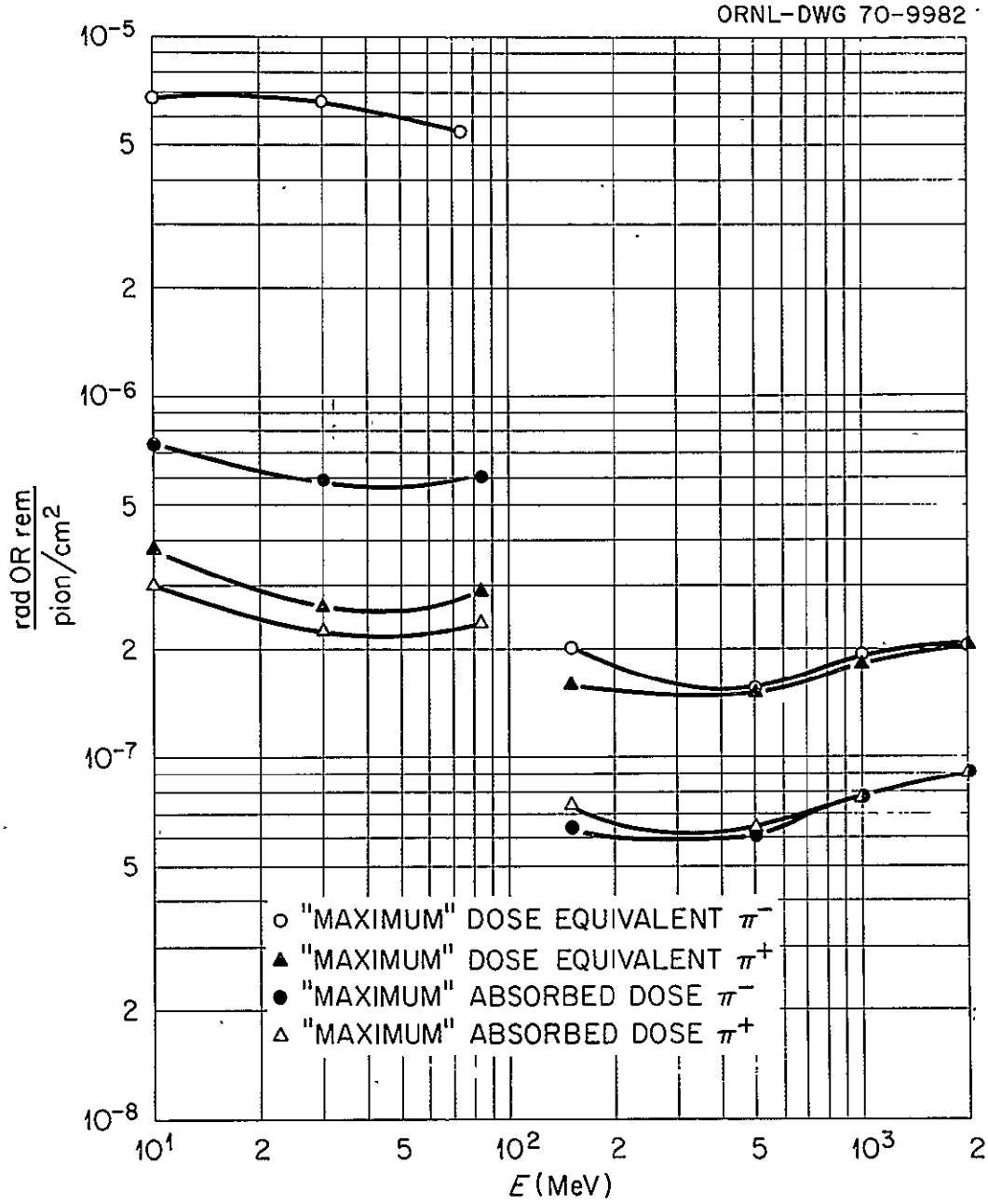

Fig. 12. "Maximum" (see discussion on pages 25 and 28) Absorbed Dose and Dose Equivalent vs Incident Pion Energy.

peaks is not known, and therefore quite different maximum values might be determined if the average were performed over a smaller depth interval. Furthermore, the position of the 1-cm interval over which the dose has been averaged with respect to the end of the pion range also has a decisive effect on the maximum value obtained; that is, the amount of energy that will be deposited in the 1-cm interval is quite dependent on where the pion stops within that interval. At energies of 150 MeV and greater, the values in Fig. 12 were obtained by drawing smooth curves by eye through the histograms in Figs. 9 and 10 and taking the maximum from each of these curves. As in Fig. 11, no curves between 84 and 150 MeV have been drawn because of the expected rapid variation of the dose values in the vicinity of 108 MeV. In Table II the quality factor obtained by dividing the maximum dose equivalent from Fig. 12 by the maximum absorbed dose from Fig. 12 is given as a function of incident energy of pions of both charges. At the lower energies, the quality factor is much larger for negative than for positive pions, but at the higher energies ($\geq$ 500 MeV) there is no appreciable difference between the quality factor for negatively and positively charged pions. The fact that the quality factor given in the table is larger for 30-MeV negative pions than that for either 10- or 84-MeV negative pions may be due to the somewhat arbitrary way in which the "maximum" is defined here and therefore may not be meaningful.

TABLE II

Quality Factor as a Function of Incident Pion Energy

Energy (MeV)	π^- Quality Factor $\frac{\text{"Maximum" Dose Equivalent}}{\text{"Maximum" Absorbed Dose}}$	π^+ Quality Factor $\frac{\text{"Maximum" Dose Equivalent}}{\text{"Maximum" Absorbed Dose}}$
10	9.1	1.2
30	11.1	1.1
84	9.2	1.2
150	3.2	2.2
500	2.6	2.3
1000	2.4	2.3
2000	2.3	2.3

APPENDIX

In this appendix the contributions to the absorbed dose and dose equivalent from the various kinds of particles produced in tissue by incident negatively and positively charged pions with energies of 10, 30, 150, 500, and 1000 MeV are given. In the figures to follow the individual contributions are defined in the same manner as in the body of the paper. The total absorbed dose and dose equivalent obtained by adding all of the contributions in a given figure are shown in the body of the paper.

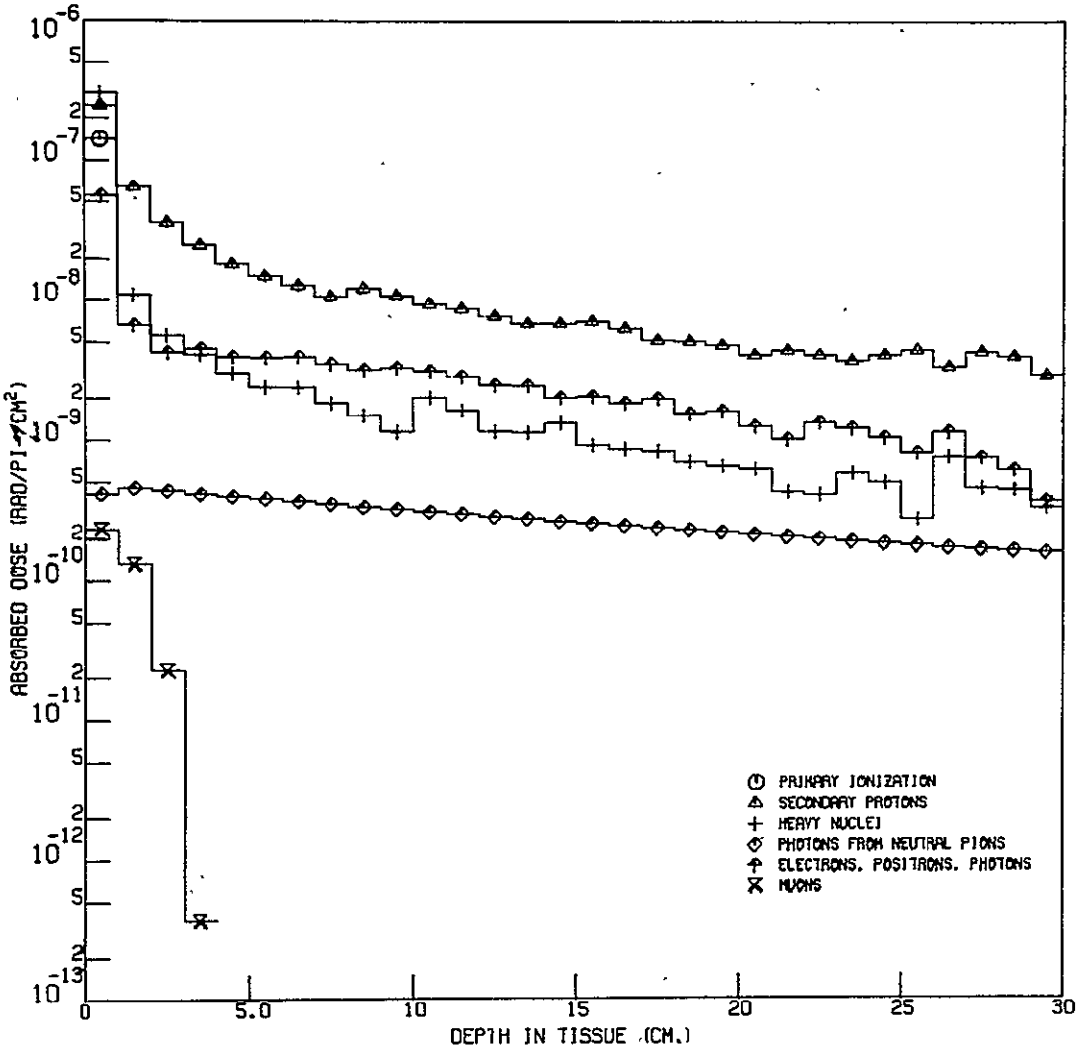

Fig. A-1. Absorbed Dose from the Various Kinds of Particles vs Depth in Tissue for 10-MeV Normally Incident Negatively Charged Pions.

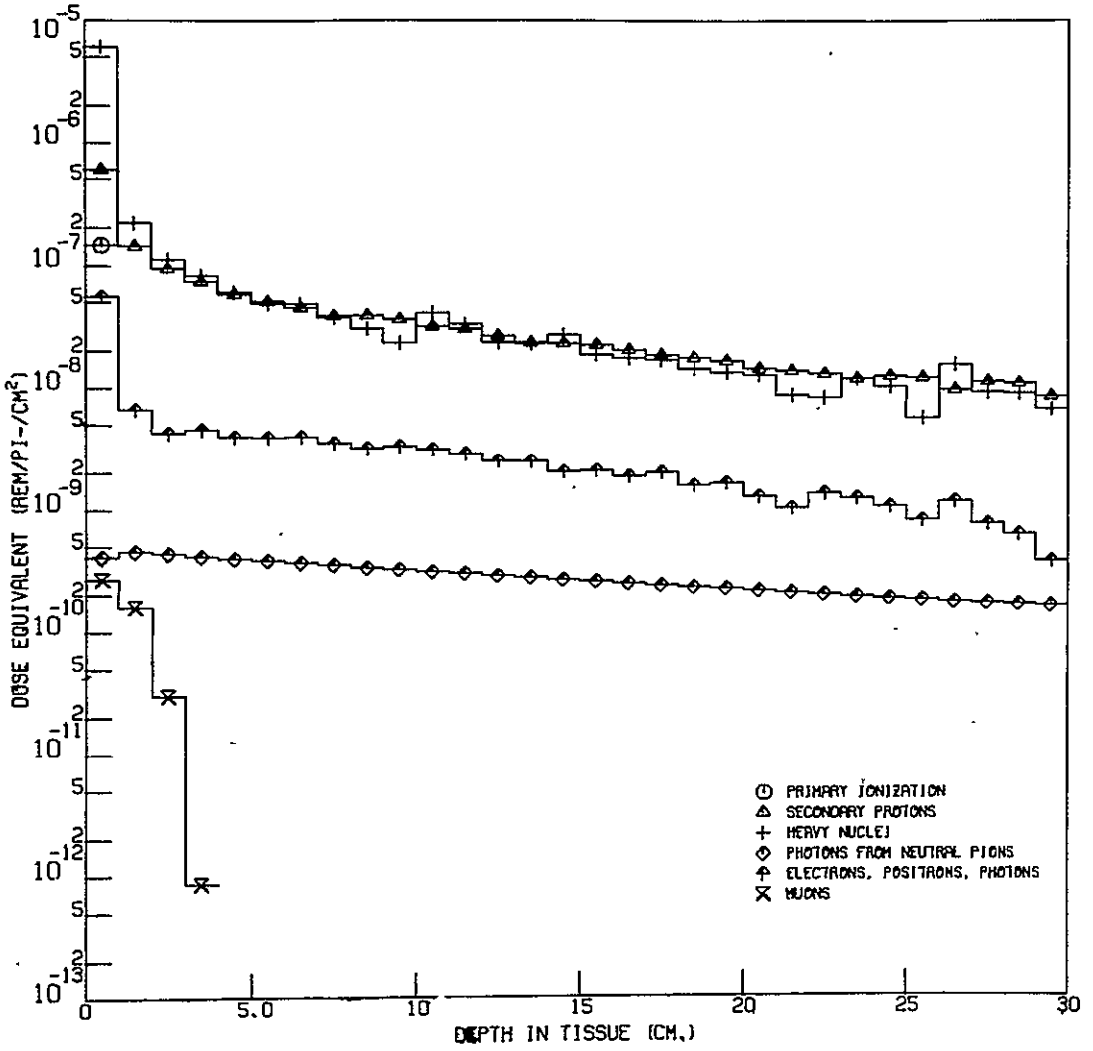

Fig. A-2. Dose Equivalent from the Various Kinds of Particles vs Depth in Tissue for 10-MeV Normally Incident Negatively Charged Pions.

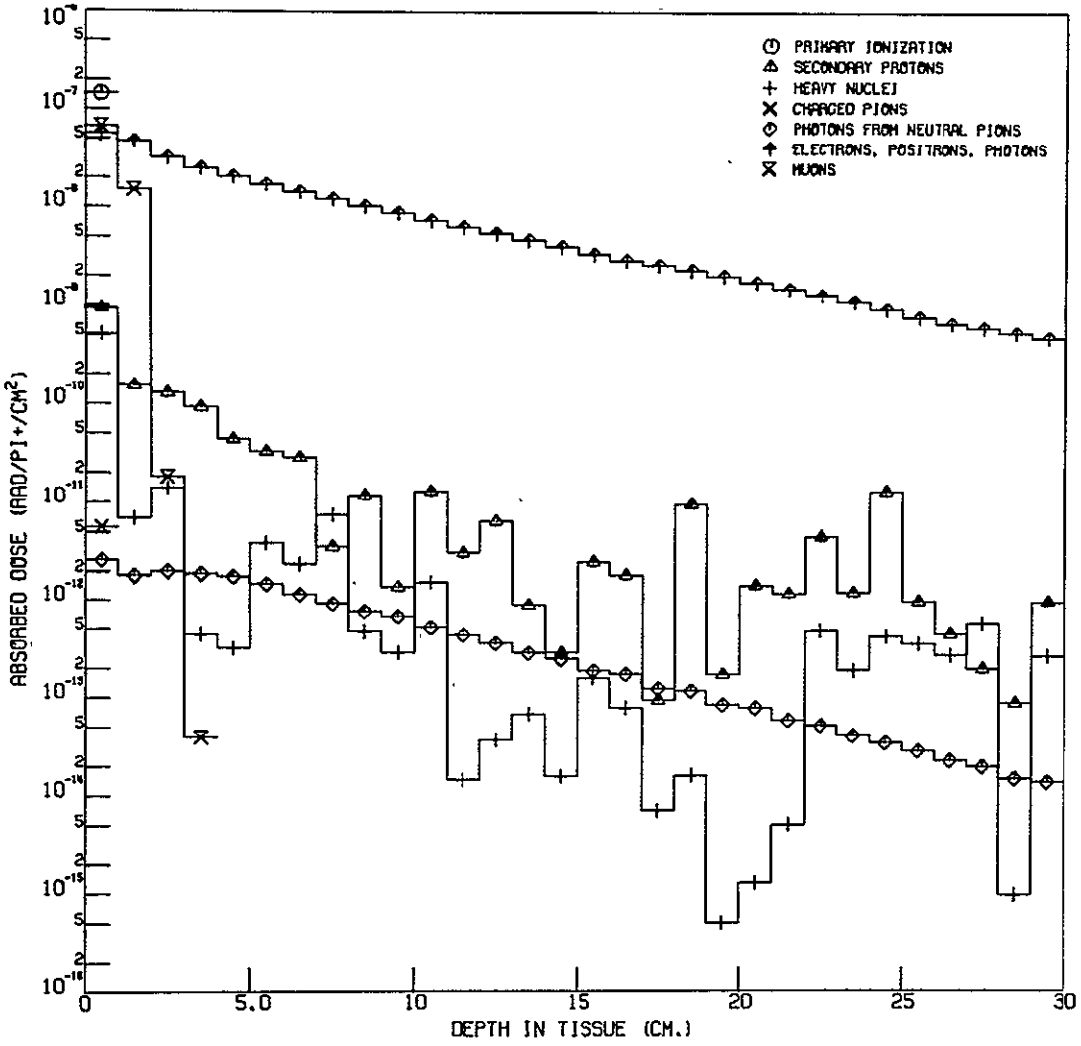

Fig. A-3. Absorbed Dose from the Various Kinds of Particles vs Depth in Tissue for 10-MeV Normally Incident Positively Charged Pions.

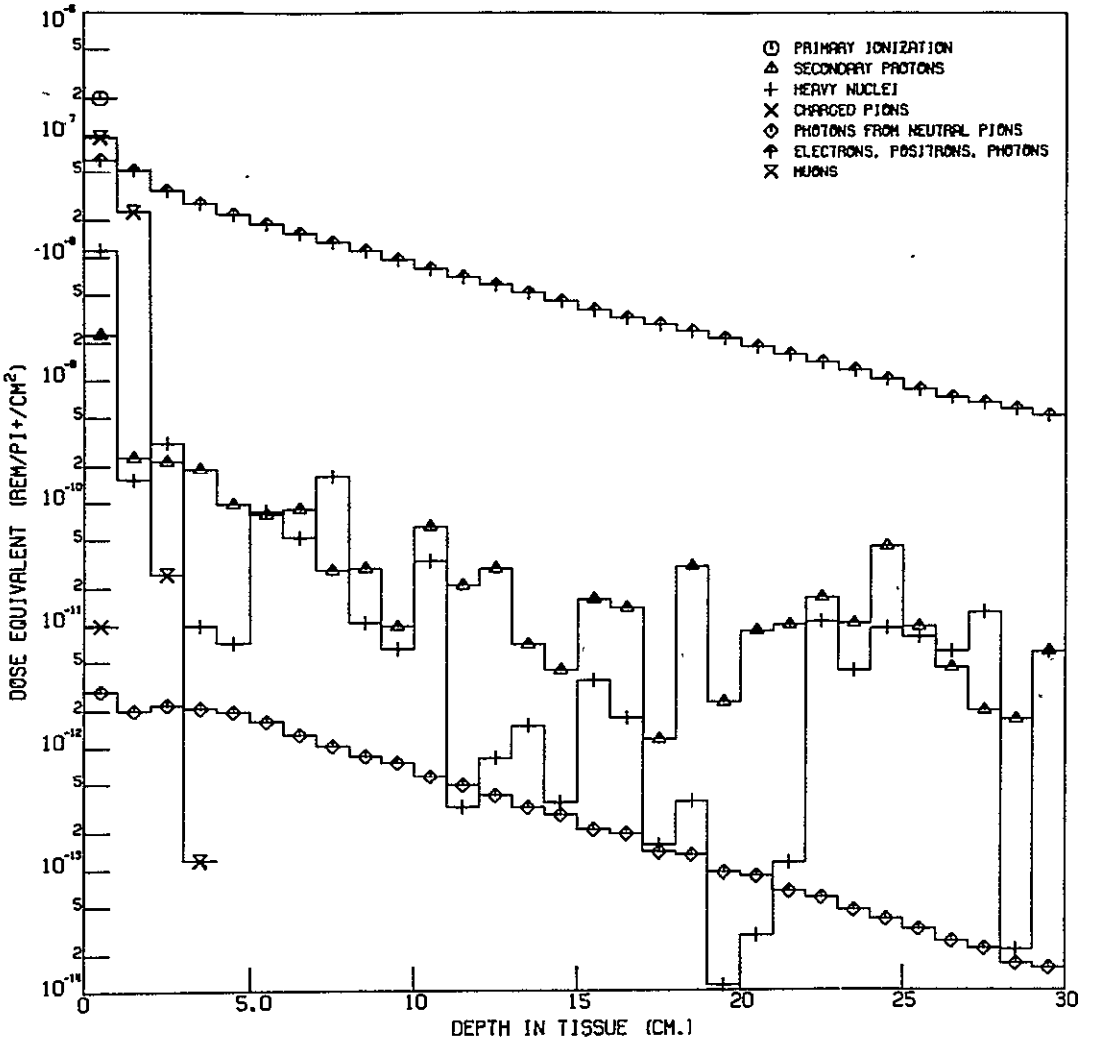

Fig. A-4. Dose Equivalent from the Various Kinds of Particles vs Depth in Tissue for 10-MeV Normally Incident Positively Charged Pions.

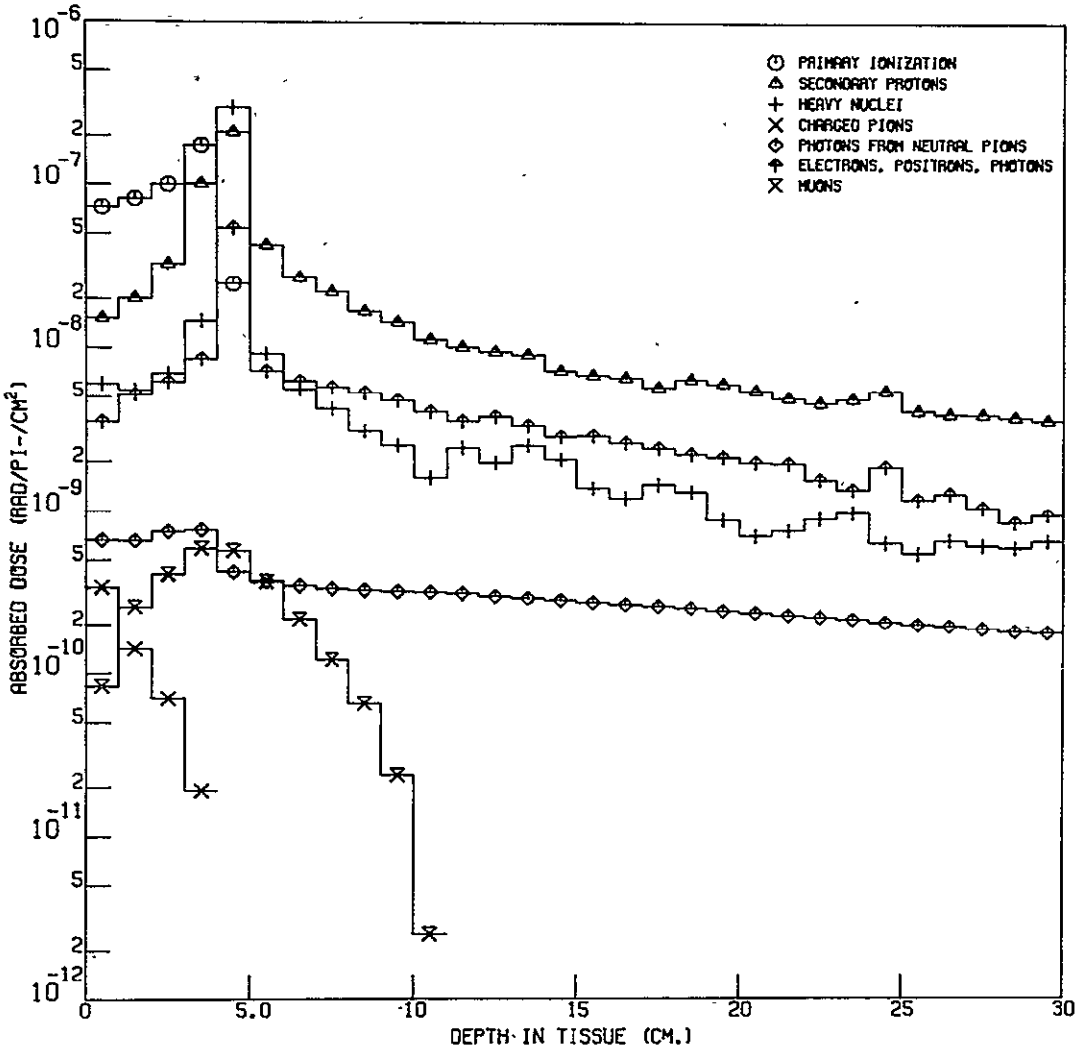

Fig. A-5. Absorbed Dose from the Various Kinds of Particles vs Depth in Tissue for 30-MeV Normally Incident Negatively Charged Pions.

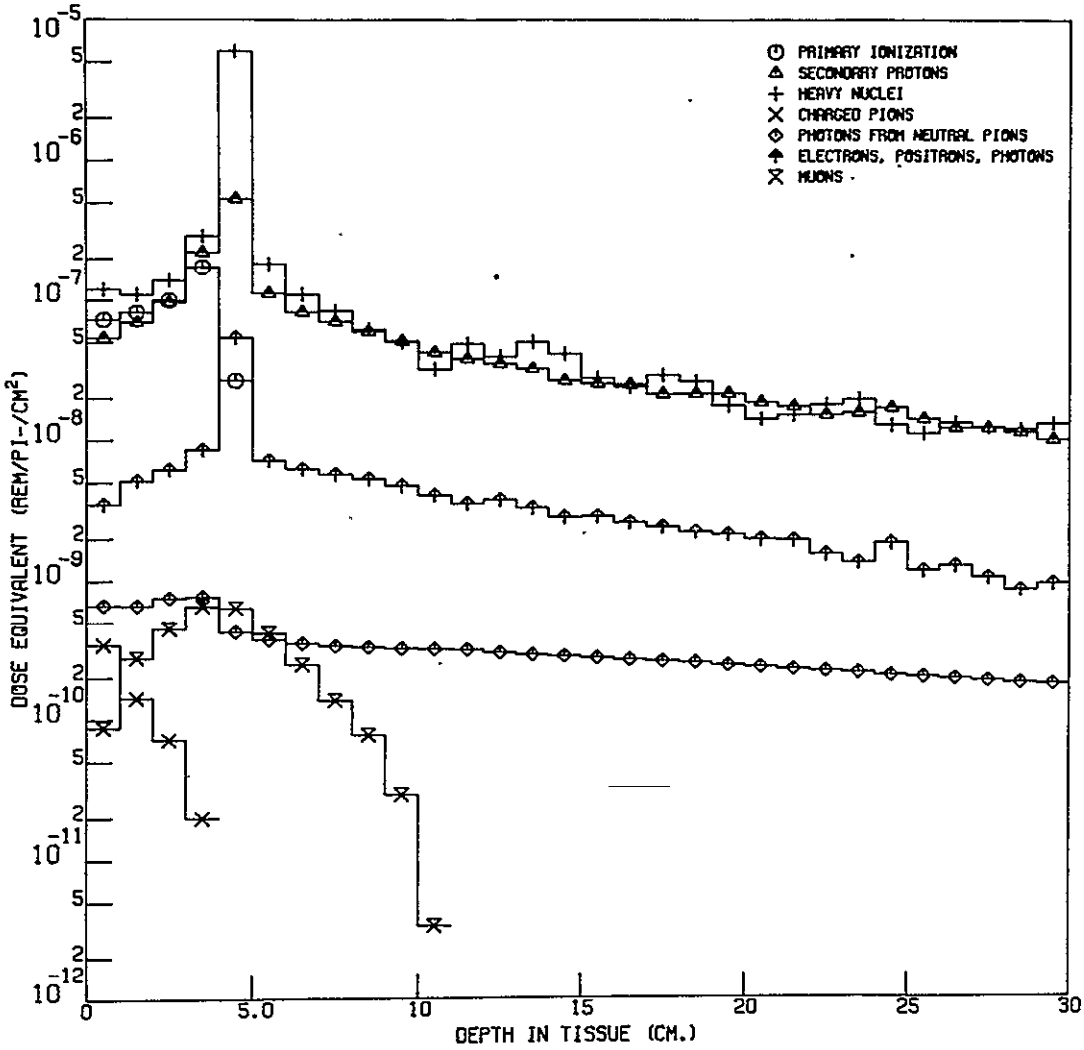

Fig. A-6. Dose Equivalent from the Various Kinds of Particles vs Depth in Tissue for 30-MeV Normally Incident Negatively Charged Pions.

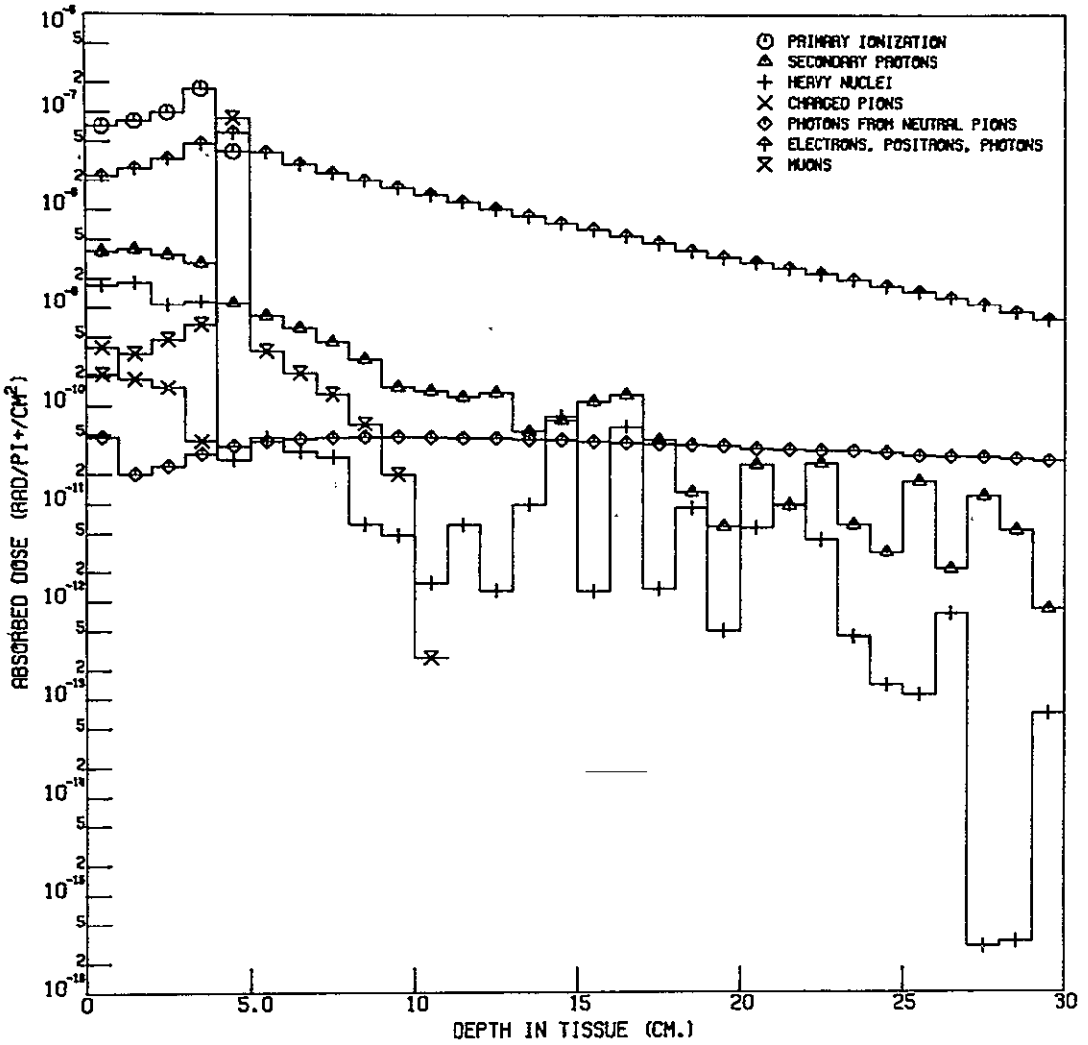

Fig. A-7. Absorbed Dose from the Various Kinds of Particles vs Depth in Tissue for 30-MeV Normally Incident Positively Charged Pions.

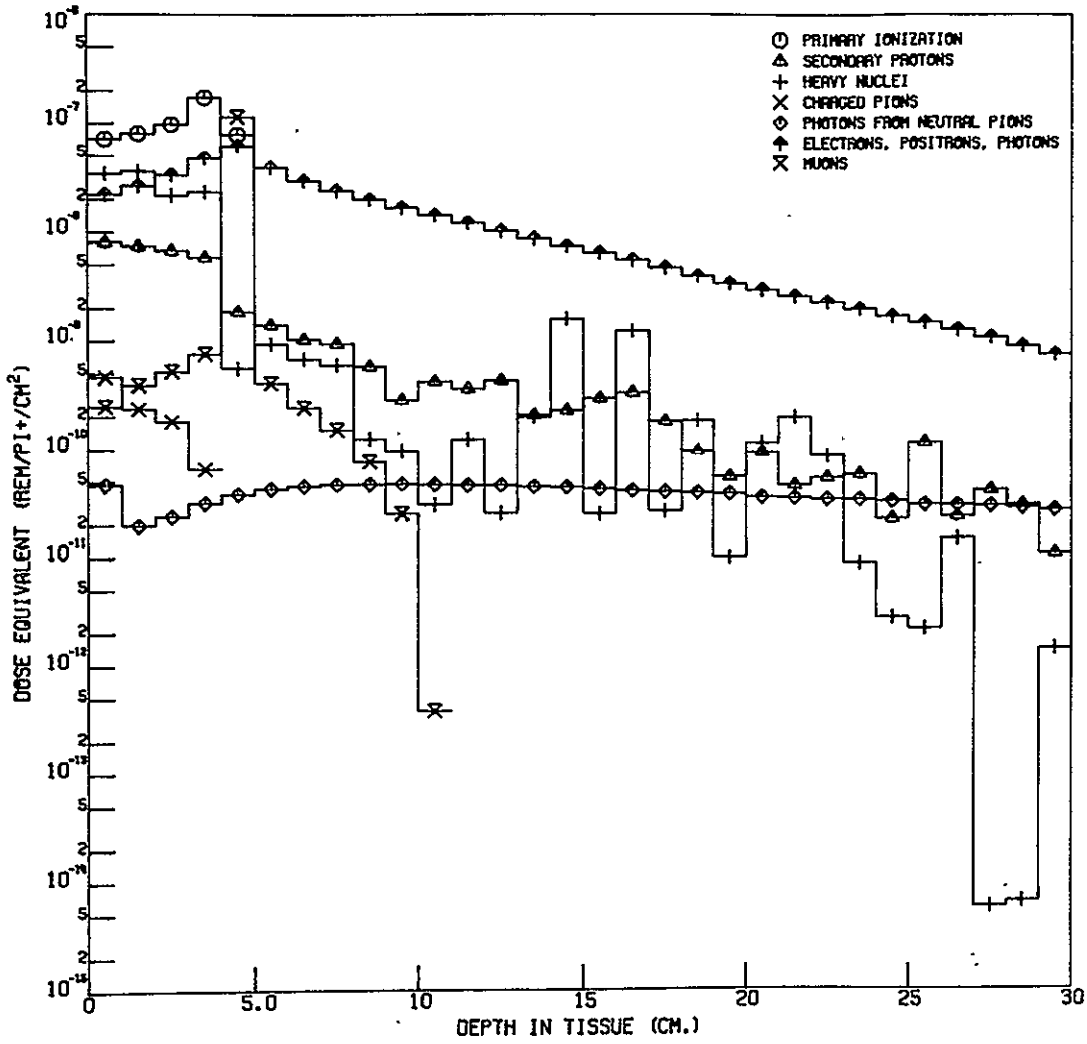

Fig. A-8. Dose Equivalent from the Various Kinds of Particles vs Depth in Tissue for 30-MeV Normally Incident Positively Charged Pions.

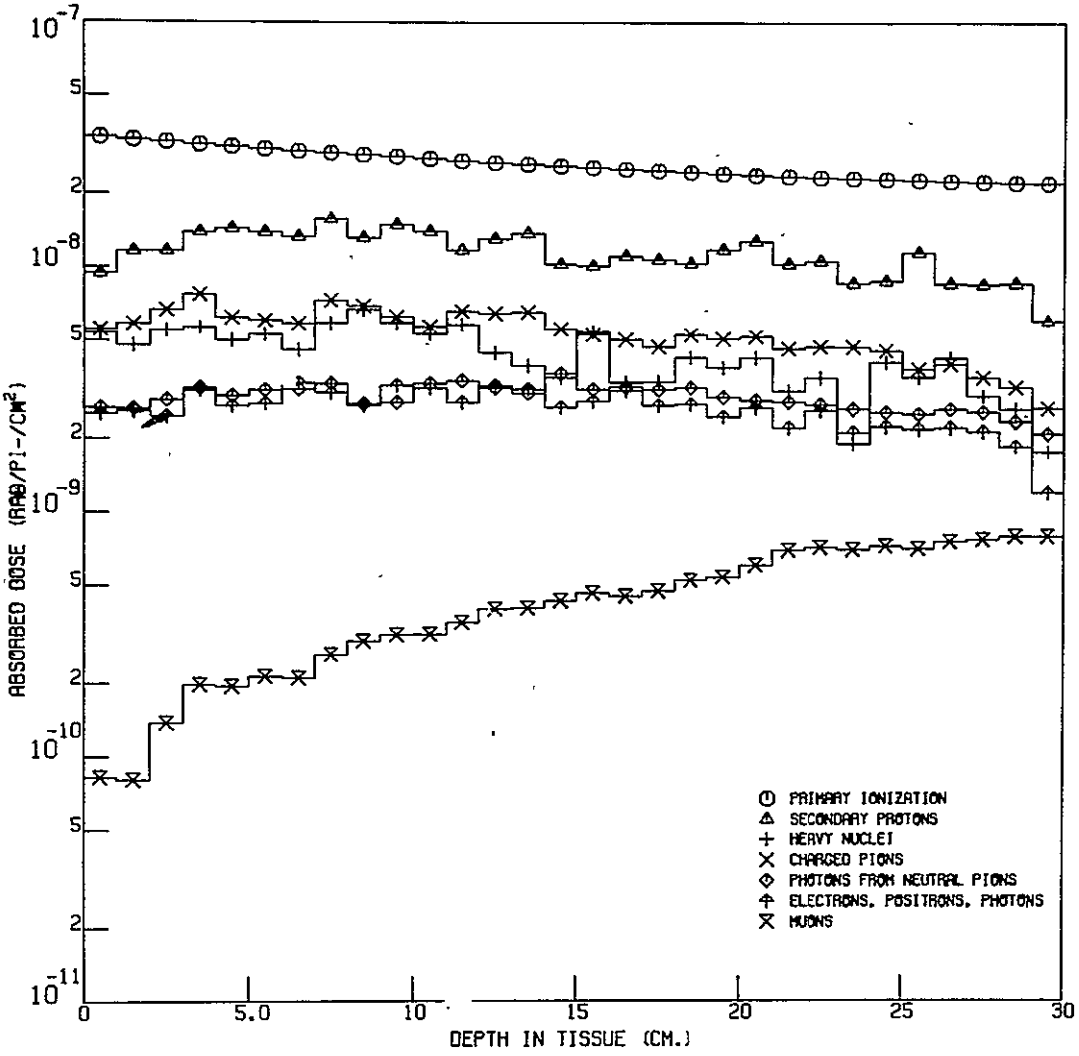

Fig. A-9. Absorbed Dose from the Various Kinds of Particles vs Depth in Tissue for 150-MeV Normally Incident Negatively Charged Pions.

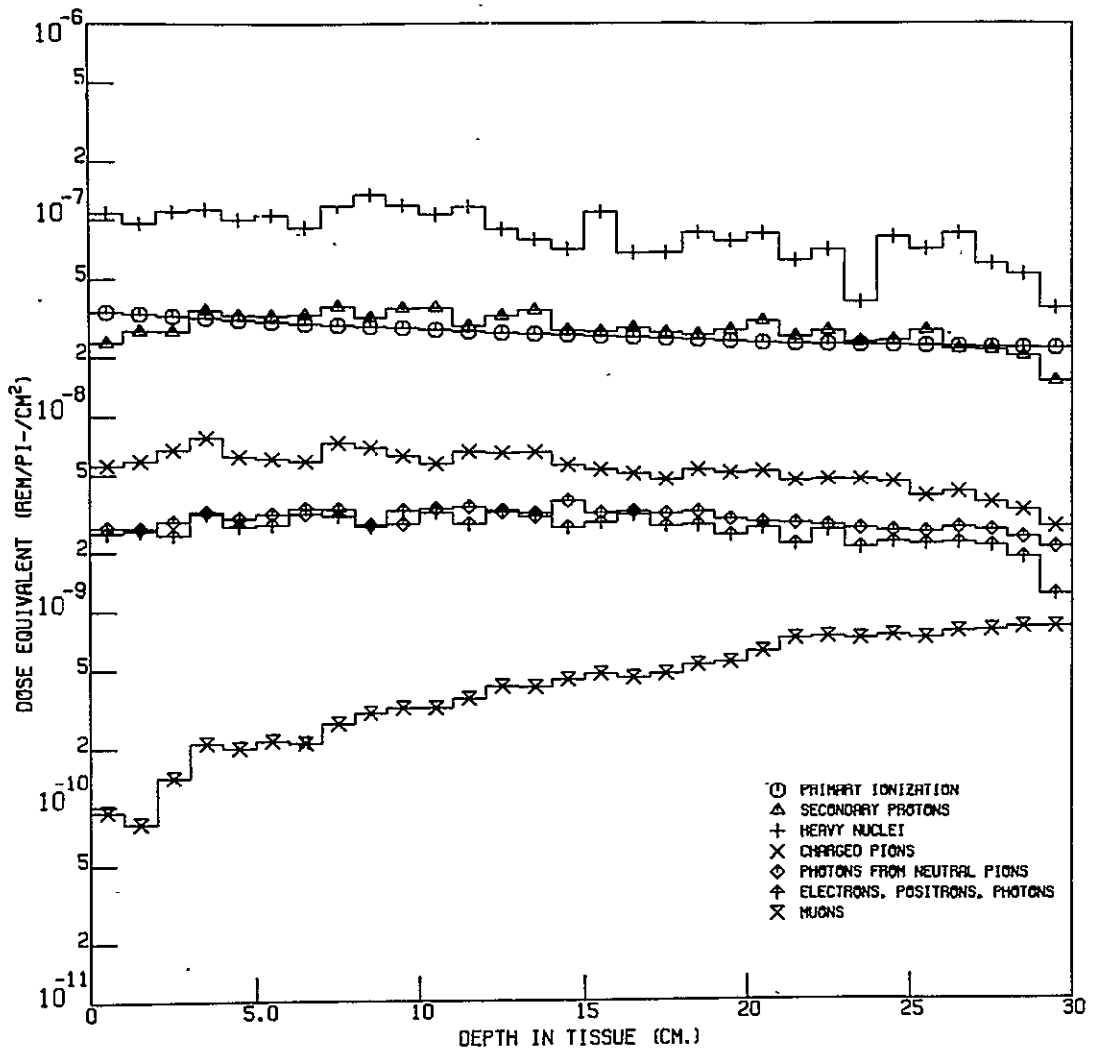

Fig. A-10. Dose Equivalent from the Various Kinds of Particles vs Depth in Tissue for 150-MeV Normally Incident Negatively Charged Pions.

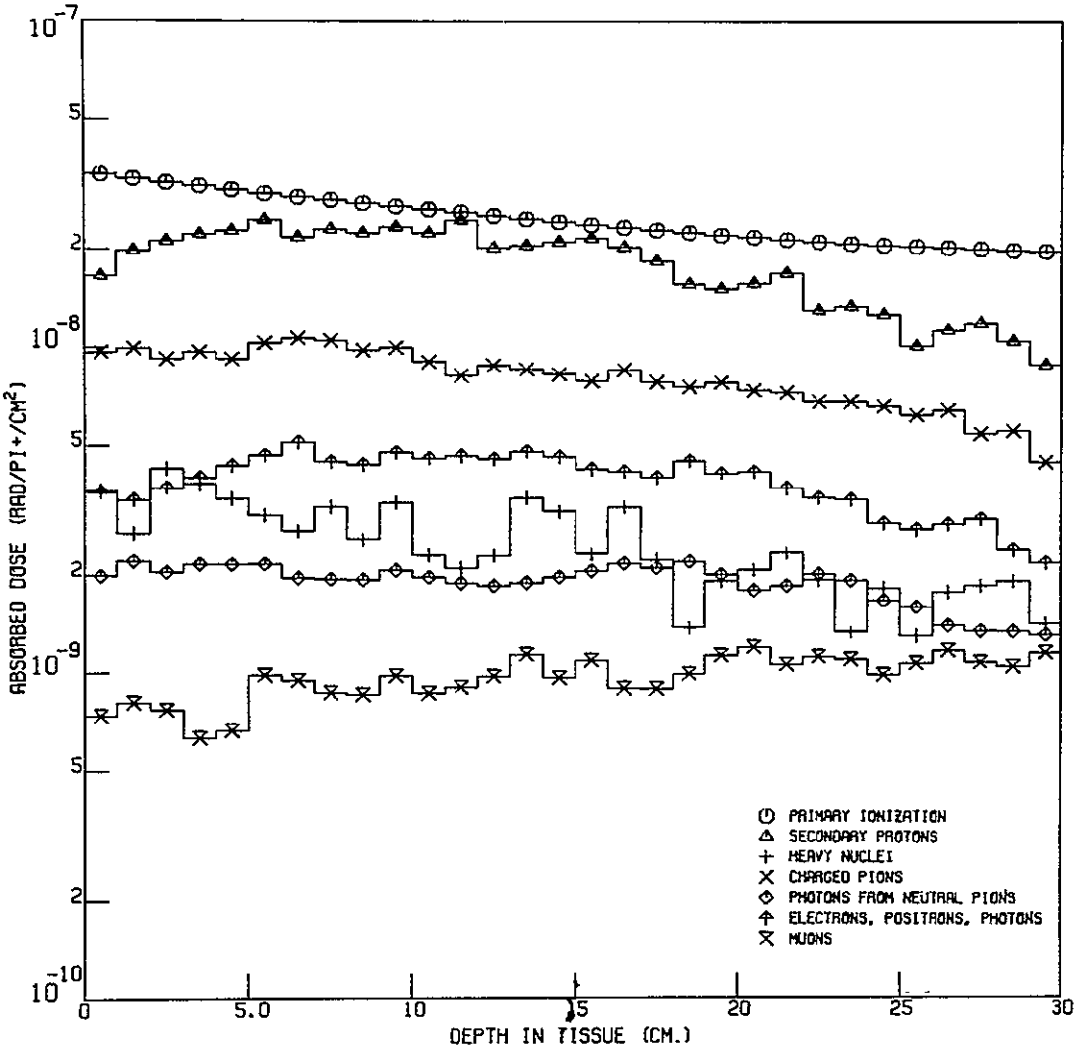

Fig. A-11. Absorbed Dose from the Various Kinds of Particles vs Depth in Tissue for 150-MeV Normally Incident Positively Charged Pions.

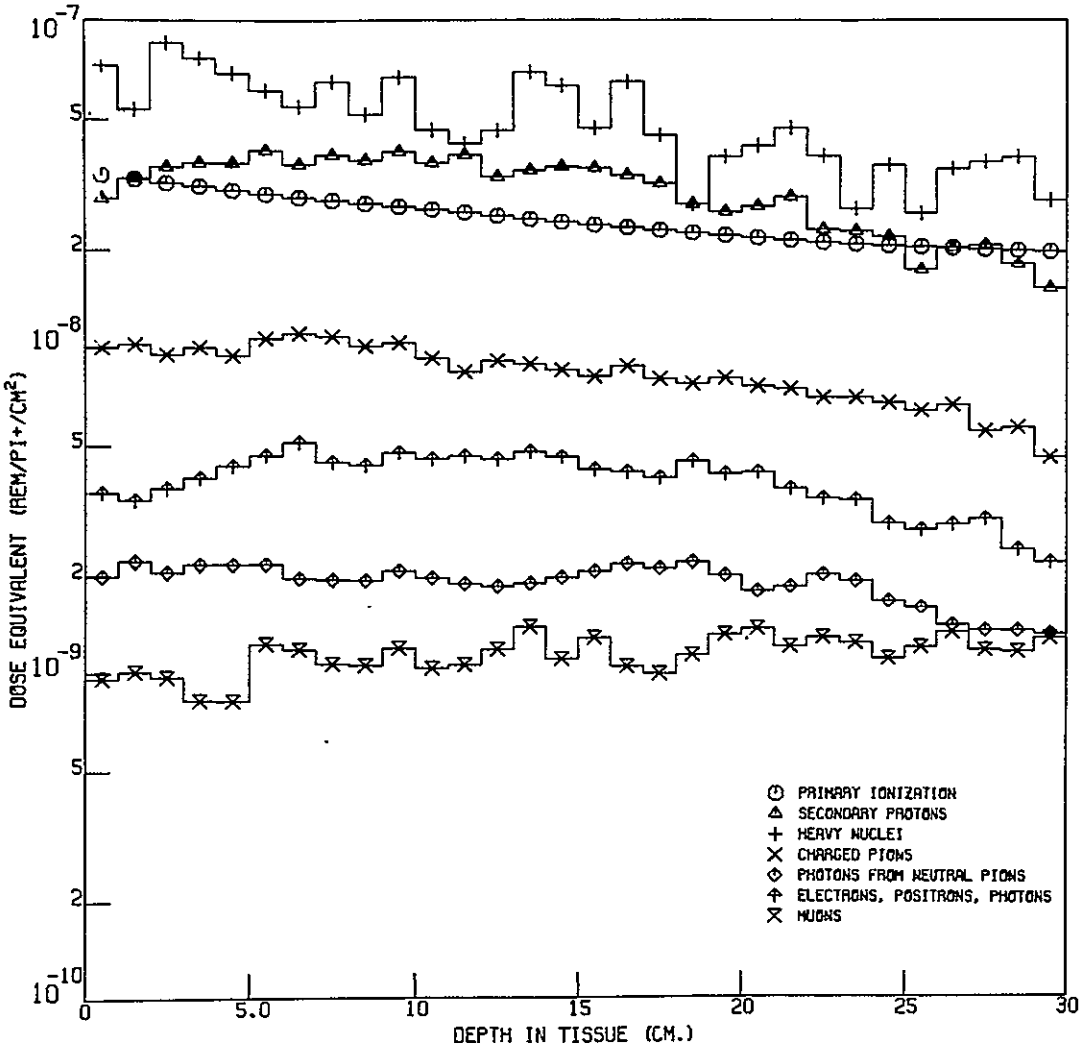

Fig. A-12. Dose Equivalent from the Various Kinds of Particles vs Depth in Tissue for 150-MeV Normally Incident Positively Charged Pions.

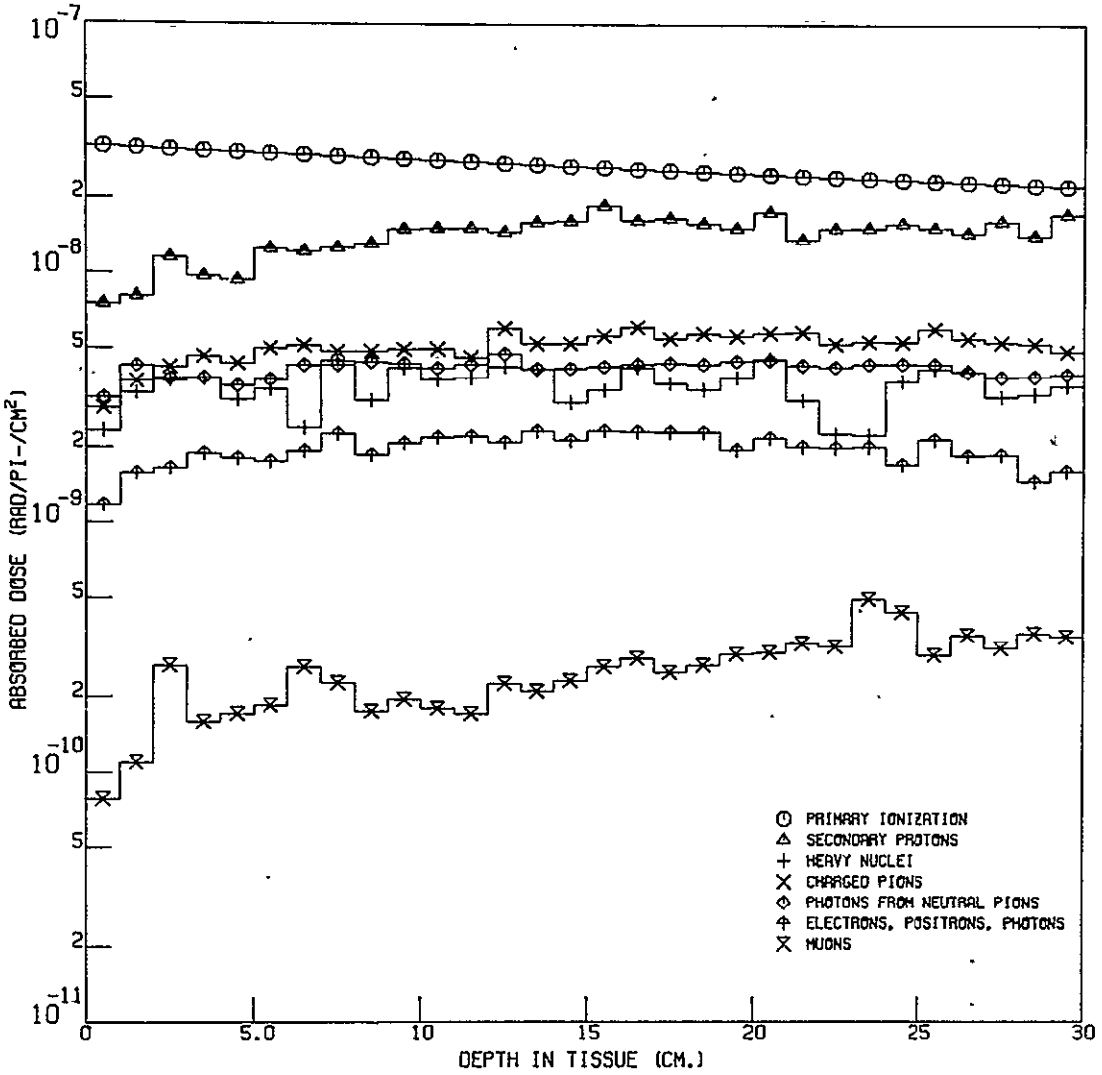

Fig. A-13. Absorbed Dose from the Various Kinds of Particles vs Depth in Tissue for 500-MeV Normally Incident Negatively Charged Pions.

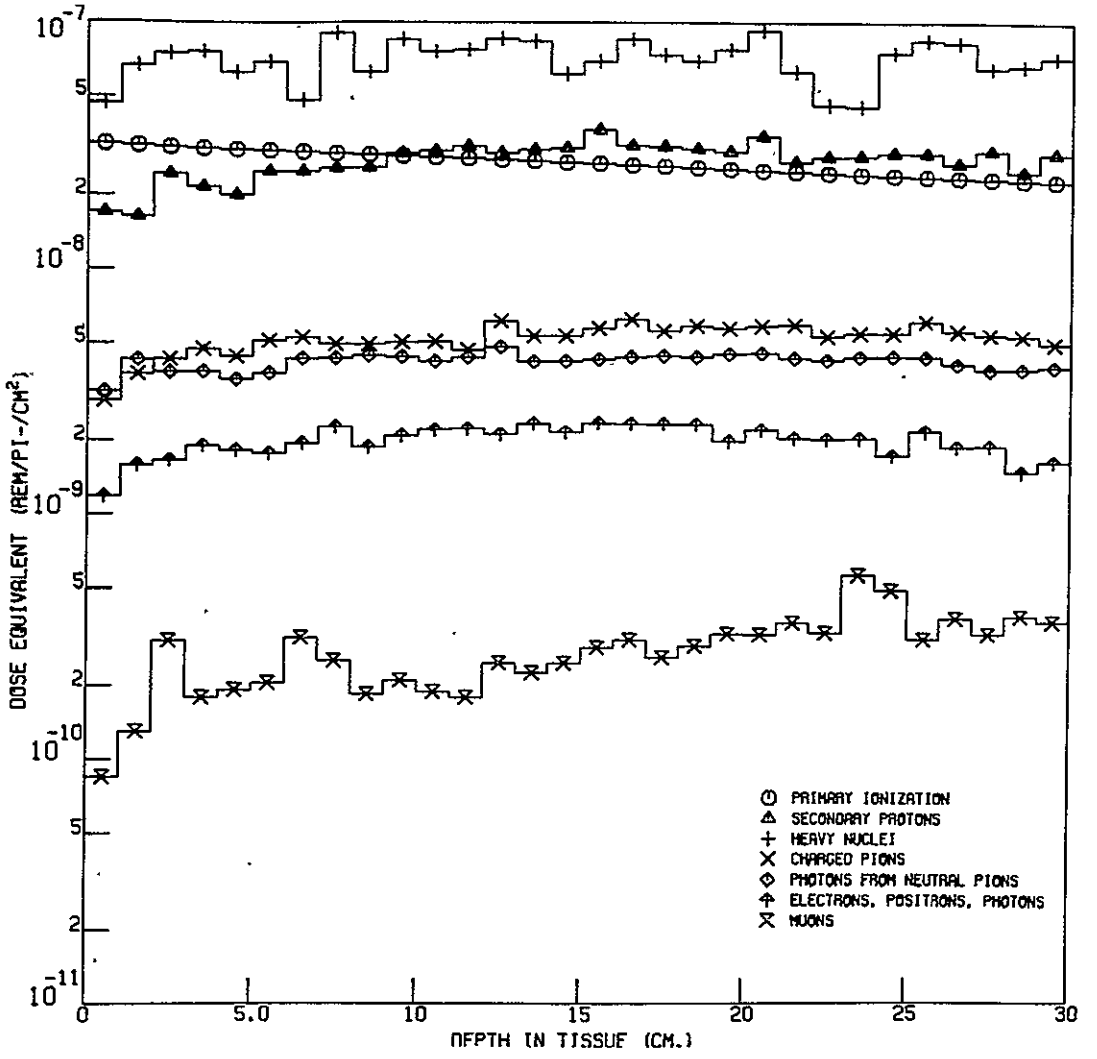

Fig. A-14. Dose Equivalent from the Various Kinds of Particles vs Depth in Tissue for 500-MeV Normally Incident Negatively Charged Pions.

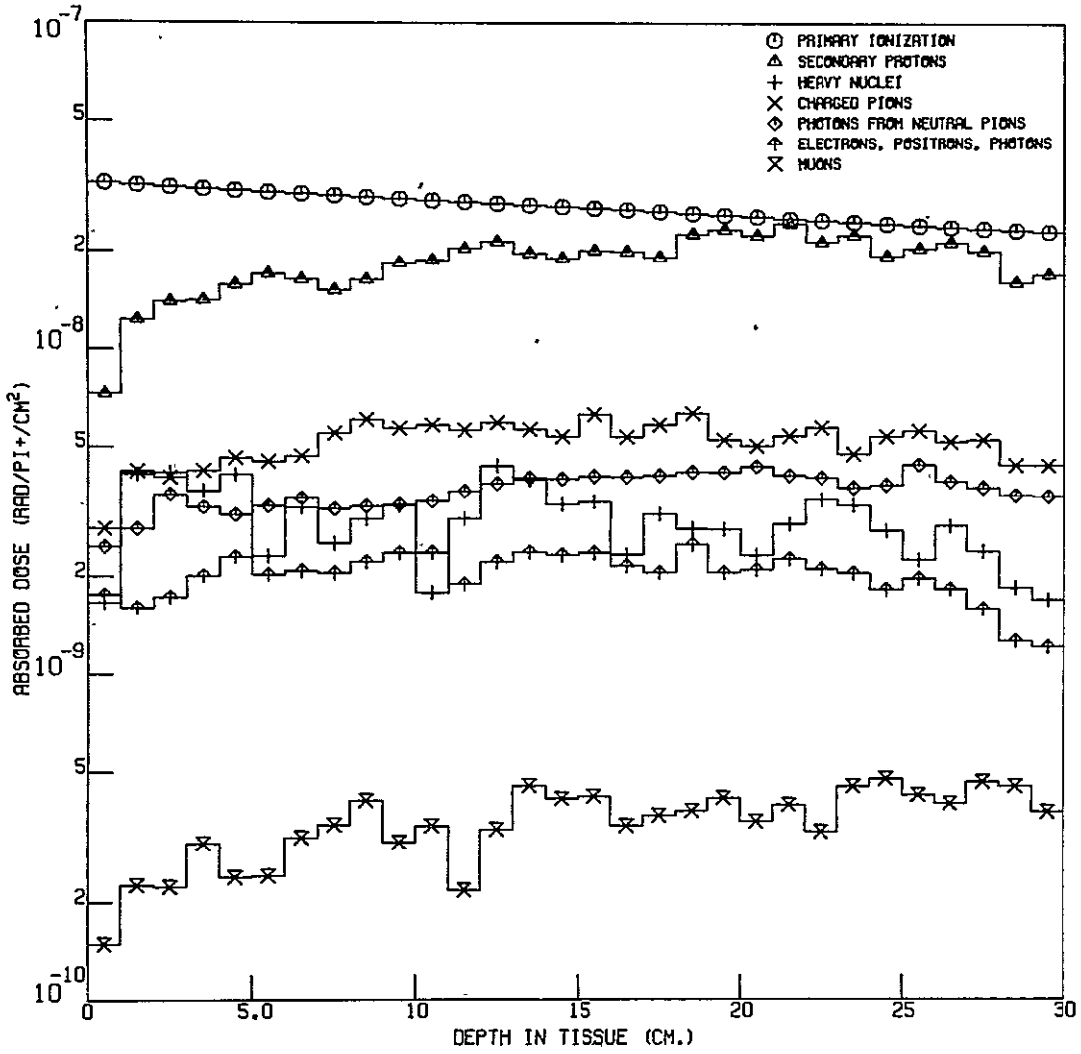

Fig. A-15. Absorbed Dose from the Various Kinds of Particles vs Depth in Tissue for 500-MeV Normally Incident Positively Charged Pions.

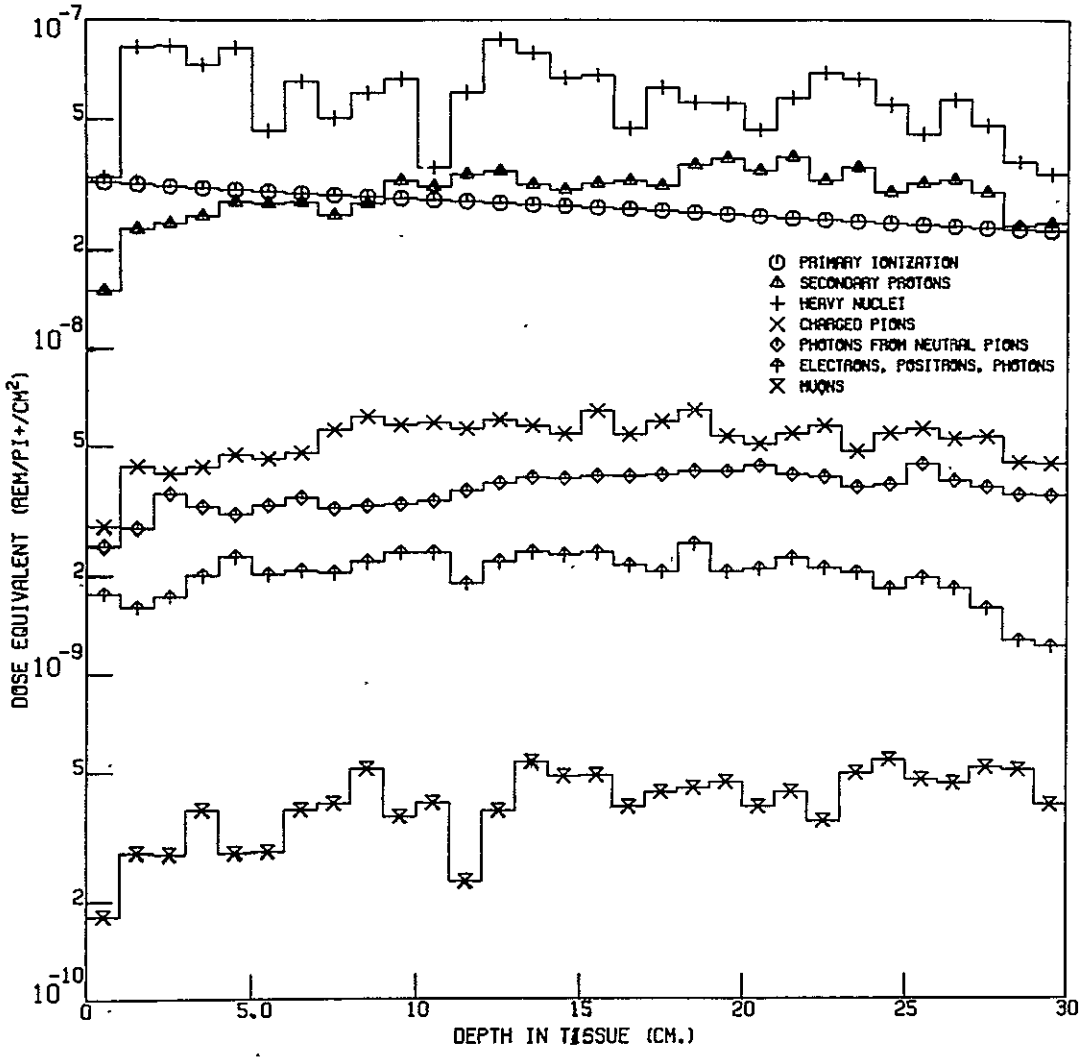

Fig. A-16. Dose Equivalent from the Various Kinds of Particles vs Depth in Tissue for 500-MeV Normally Incident Positively Charged Pions.

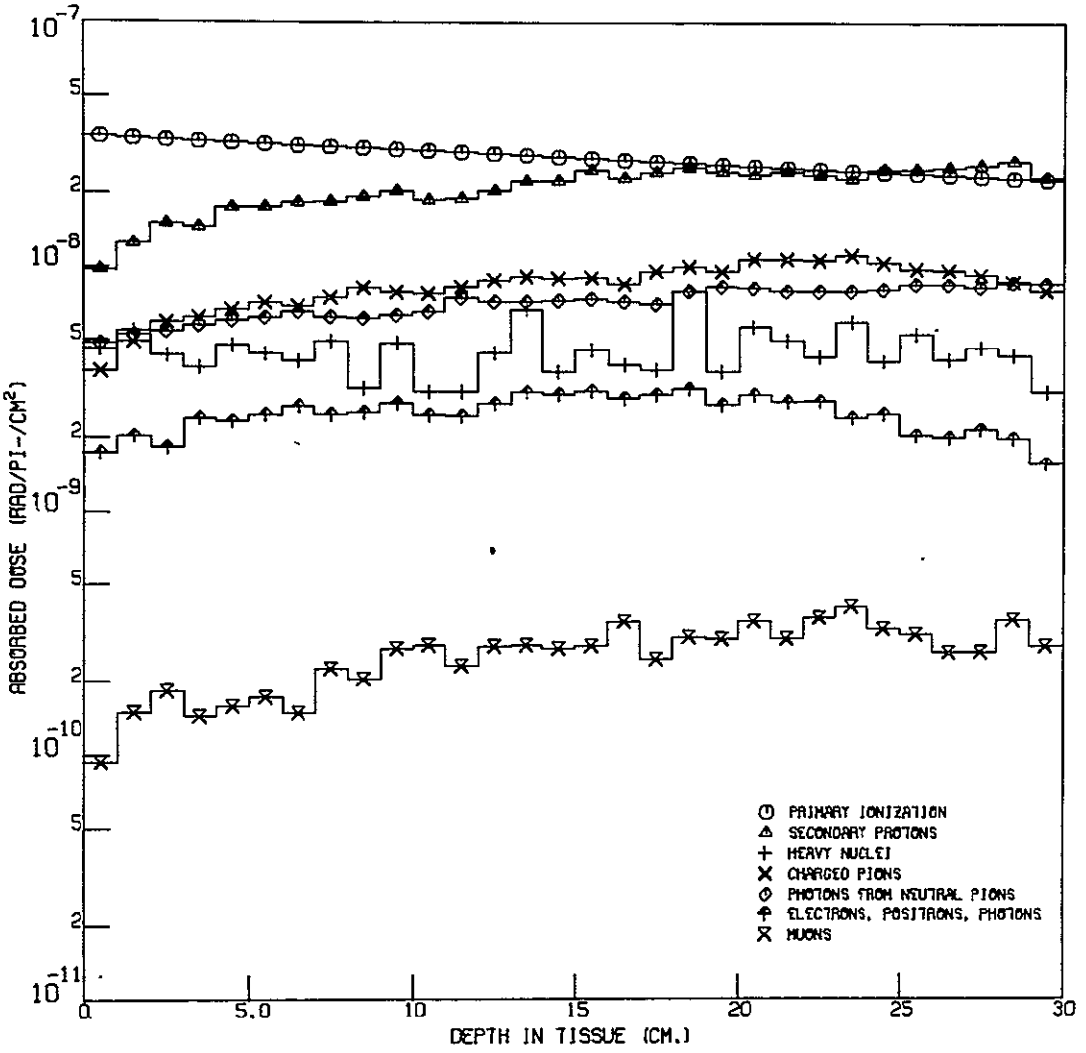

Fig. A-17. Absorbed Dose from the Various Kinds of Particles vs Depth in Tissue for 1000-MeV Normally Incident Negatively Charged Pions.

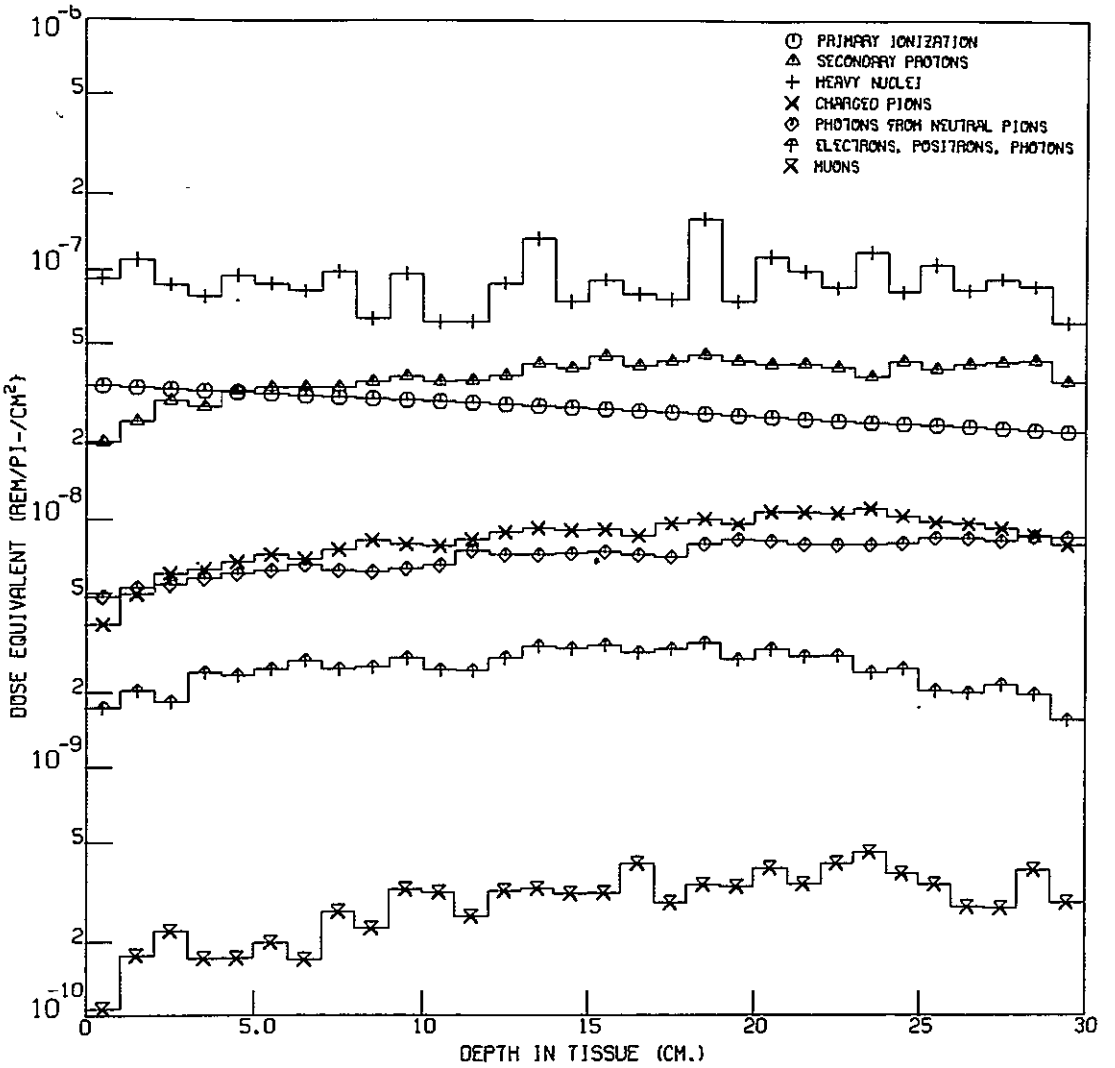

Fig. A-18. Dose Equivalent from the Various Kinds of Particles vs Depth in Tissue for 1000-MeV Normally Incident Negatively Charged Pions.

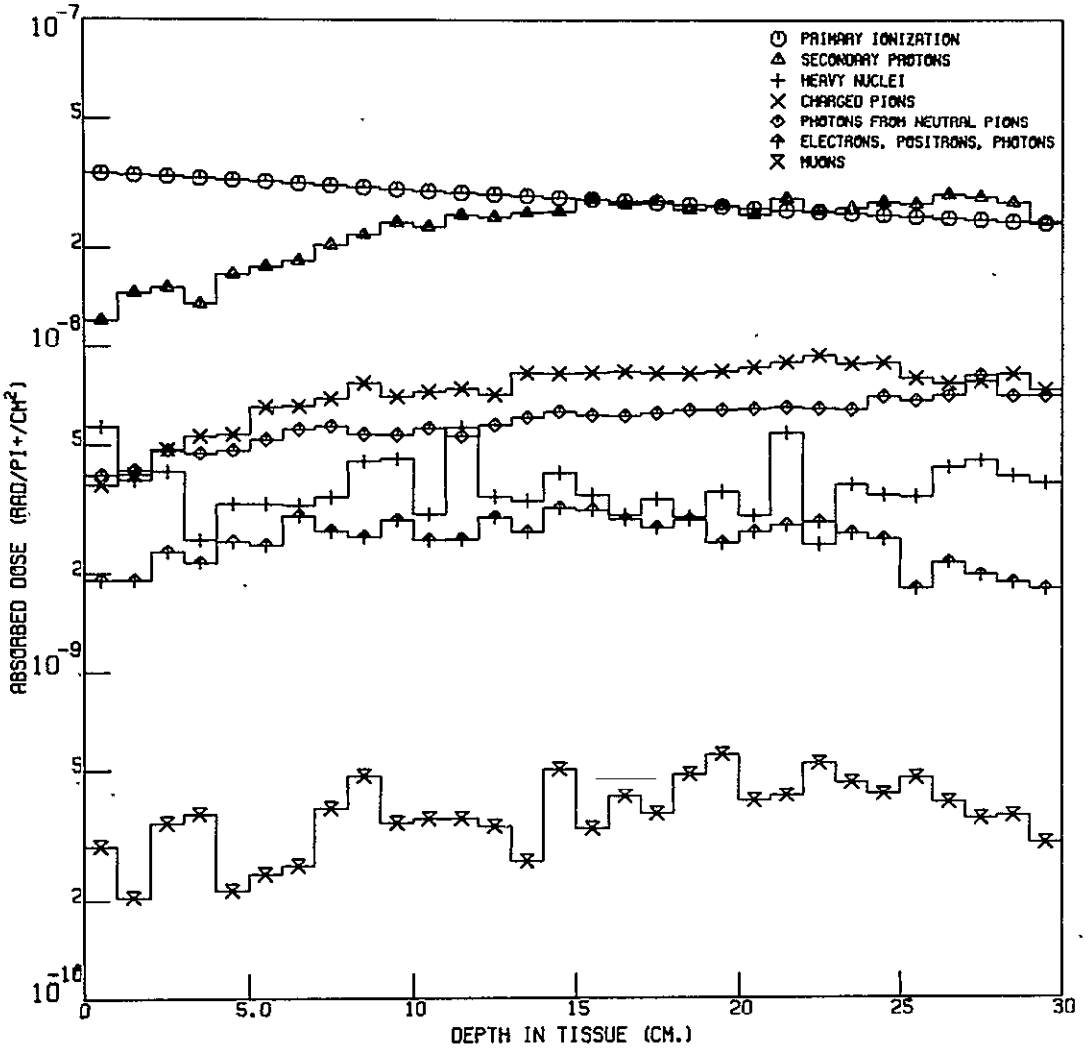

Fig. A-19. Absorbed Dose from the Various Kinds of Particles vs Depth in Tissue for 1000-MeV Normally Incident Positively Charged Pions.

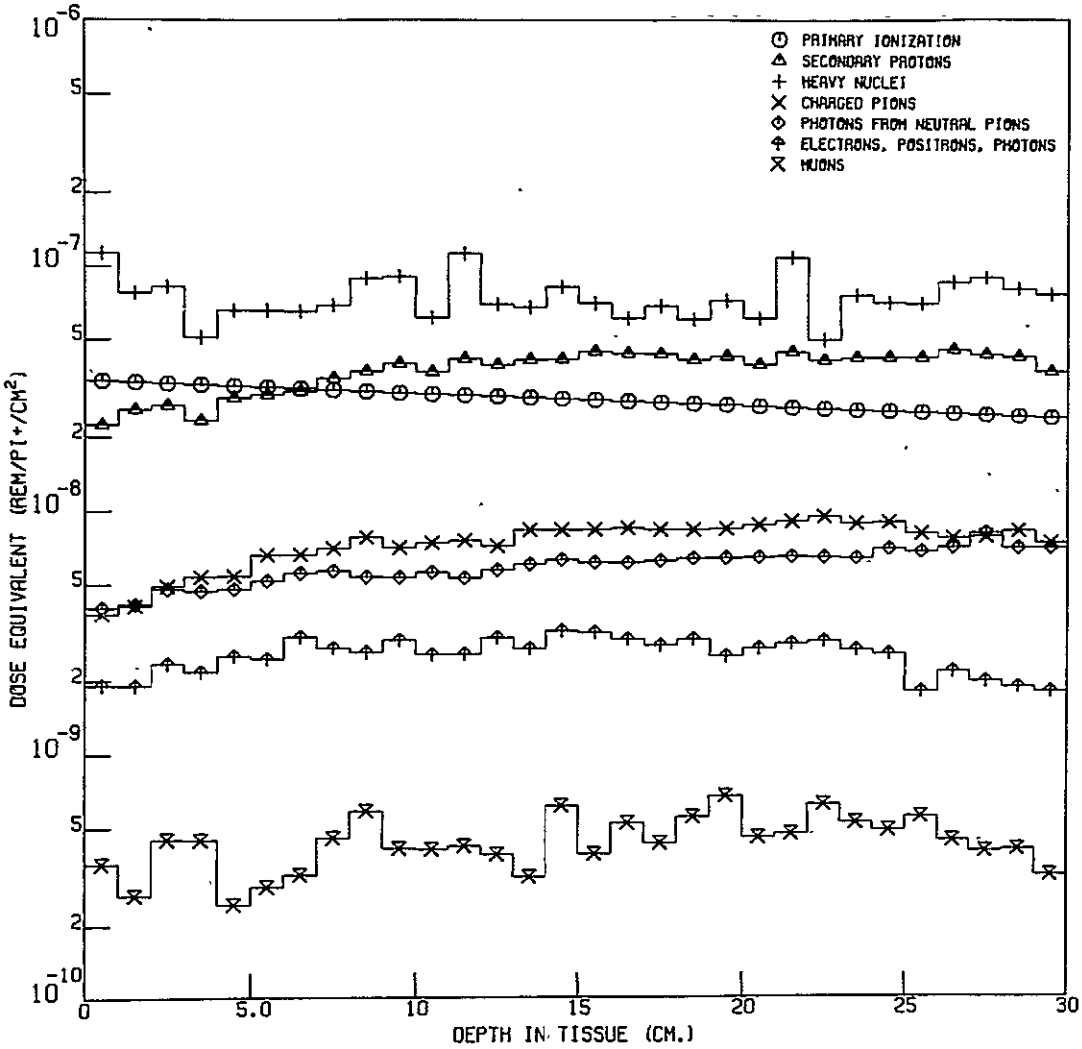

Fig. A-20. Dose Equivalent from the Various Kinds of Particles vs Depth in Tissue for 1000-MeV Normally Incident Positively Charged Pions.

FOOTNOTES

a. This cross-section tape, together with references to all of the data used, is available on request from the Radiation Shielding Information Center of the Oak Ridge National Laboratory.

b. Experimental data for the absorbed dose from 84-MeV incident negatively and positively charged pions are available,[24] but because the experimental geometry was not that of a very broad beam incident on a semi-infinite slab of tissue, a meaningful comparison between these data and the results presented here could not be obtained.

c. Results similar to those shown in Figs. 1 to 8 for all of the incident pion energies considered in this paper are given in the Appendix.

d. References to the experimental data used for these cross sections, as well as graphs of the cross sections used in the calculations, may be found in ref. 12.

REFERENCES

1. R. G. ALSMILLER, Jr., T. W. ARMSTRONG, and W. A. COLEMAN, "The Absorbed Dose and Dose Equivalent from Neutrons in the Energy Range 60 to 3000 MeV and Protons in the Energy Range 400 to 3000 MeV," ORNL-TM-2924, Oak Ridge National Laboratory (1970); to be published in Nucl. Sci. Eng.
2. P. H. FOWLER and D. H. PERKINS, Nature 189, 524 (1961).
3. P. H. FOWLER, Proc. Phys. Soc. 85, 1051 (1965).
4. L. ROSEN, Nucl. Appl. 5, #6, 379 (1968).
5. W. A. COLEMAN and R. G. ALSMILLER, Jr., Nucl. Sci. Eng. 34, 104 (1968); see also ORNL-TM-2206, Oak Ridge National Laboratory (1968).
6. H. BETHE and J. ASHKIN, "Passage of Radiation Through Matter," Experimental Nuclear Physics, ed. E. Segre, Part II, John Wiley & Sons, Inc., New York (1963).
7. T. W. ARMSTRONG and R. G. ALSMILLER, Jr., Nucl. Instr. Meth. 82, 289 (1970).
8. H. W. BERTINI, Phys. Rev. 188, 1711 (1969).
9. H. W. BERTINI, Phys. Rev. 131, 1801 (1963); with erratum, Phys. Rev. 138, AB2 (1965).
10. H. W. BERTINI, Nucl. Phys. 87, 138 (1966).
11. M. P. GUTHRIE, "EVAP-2 and EVAP-3: Modifications of a Code to Calculate Particle Evaporation from Excited Compound Nuclei," ORNL-4379, Oak Ridge National Laboratory (1969).
12. H. W. BERTINI, "Monte Carlo Calculations on Intranuclear Cascades," ORNL-3383, Oak Ridge National Laboratory (1963).
13. M. P. GUTHRIE, R. G. ALSMILLER, Jr., and H. W. BERTINI, Nucl. Instr. Meth. 66, 29 (1968).

14. JOSEPH H. SCANLON and S. N. MILFORD, "Cosmic Ray Collisions in Space. Part I - The Energy Spectra of Electrons From Pion-Muon-Electron Decays in Interstellar Space," NASA CR-148, Grumman Aircraft Engineering Corporation (1965).

15. C. D. ZERBY and H. S. MORAN, "Studies of the Longitudinal Development of High-Energy Electron-Photon Cascade Showers in Copper," ORNL-3329, Oak Ridge National Laboratory (1962).

16. C. D. ZERBY and H. S. MORAN, "A Monte Carlo Calculation of the Three-Dimensional Development of High-Energy Electron-Photon Cascade Showers," ORNL-TM-422, Oak Ridge National Laboratory (1962).

17. R. G. ALSMILLER, Jr. and H. S. MORAN, Nucl. Sci. Eng. 38, 131 (1969).

18. R. G. ALSMILLER, Jr. and H. S. MORAN, Nucl. Sci. Eng. 40, 483 (1970).

19. H. L. BECK, Nucl. Instr. Meth. 78, 333 (1970).

20. H. C. CLAIBORNE and D. K. TRUBEY, "Dose Rates in a Slab Phantom From Monoenergetic Gamma Rays," ORNL-TM-2574, Oak Ridge National Laboratory (1969).

21. Y. SHIMA and R. G. ALSMILLER, Jr., Nucl. Sci. Eng. 41, 47 (1970).

22. C. D. ZERBY and W. E. KINNEY, Nucl. Instr. Meth. 36, 125 (1965).

23. J. E. TURNER *et al.*, Health Phys. 10, 783 (1964).

24. A. H. SULLIVAN and J. BAARLI, Phys. Med. Biol. 13, 435 (1968).

25. B. ROSSI, High-Energy Particles, Prentice-Hall, Inc., Englewood Cliffs, N. J. (1956).

Internal Distribution

1-3. L. S. Abbott
4. F. S. Alsmiller
5-24. R. G. Alsmiller, Jr.
25-29. T. W. Armstrong
30. H. W. Bertini
31. B. L. Bishop
32. C. E. Clifford
33. T. A. Gabriel
34. M. P. Guthrie
35. W. E. Kinney
36. T. A. Love
37. F. C. Maienschein
38. R. W. Peelle
39. R. W. Roussin
40. R. T. Santoro
41. D. Sundberg
42. D. K. Trubey
43. J. W. Wachter
44. H. A. Wright
45. W. Zobel
46. E. R. Cohen (consultant)
47. H. Feshbach (consultant)
48. H. Goldstein (consultant)
49. C. R. Mehl (consultant)
50-51. Central Research Library
52. ORNL Y-12 Technical Library, Document Reference Section
53-54. Laboratory Records Department
55. Laboratory Records ORNL RC
56. ORNL Patent Office

External Distribution

57. P. B. Hemmig, Division of Reactor Development & Technology, U. S. Atomic Energy Commission, Washington, D. C.
58. W. H. Hannum, Division of Reactor Development & Technology, U. S. Atomic Energy Commission, Washington, D. C.
59. Kermit Laughon, AEC Site Representative.
60. W. A. Coleman, Science Applications, Inc., P. O. Box 2351, La Jolla, California, 92037.
61-185. Given NASA Space and AEC High-Energy Accelerator Shielding Distribution*
186-200. Division of Technical Information (DTIE).
201. Laboratory and University Division (ORO).

*This distribution list is available upon request.